NASA Contractor Report 159239

Vibration Analysis of the Long Duration Exposure Facility (LDEF) Using SPAR

Harold Edighoffer

General Electric Company
Philadelphia, PA 19101

Contract NAS1-14375-15
June 1980

National
Aeronautics and
Space
Administration

Langley Research Center
Hampton, VA 23665

VIBRATION ANALYSIS OF THE LONG DURATION EXPOSURE FACILITY USING SPAR

By

Harold H. Edighoffer
General Electric Company
Philadelphia, PA 19101

Contract NAS1-14375-15
1980

This paper presents a structural dynamic modeling of the Long Duration Exposure Facility (LDEF), which is a Space Shuttle payload of passive scientific experiments contained in trays mounted on a large cylindrically shaped structure. Special detailed finite element modeling, using the SPAR system of computer programs, was required to obtain good agreement between analytical and test vibration modes. The scientific experiment trays contributed significantly to overall LDEF stiffnesses, and these contributions were realistically represented for each tray by the stiffness matrix of an equivalent orthotropic panel in the overall LDEF model. Orthotropic stiffnesses for this equivalent panel were obtained from finely detailed statically loaded SPAR models which included stiffness coupling and allowed for partial relative sliding of the tray clamping attachments. Sensitivity to LDEF joint boundary conditions was determined, and static test data proved valuable in assessing modeling of local end fittings.

TABLE OF CONTENTS

	Page
LIST OF FIGURES	v
LIST OF TABLES	vii
SUMMARY	1
INTRODUCTION	2
SYMBOLS	3
LDEF STRUCTURAL TEST CONFIGURATION	8
SPAR LDEF MODEL	18
Longerons and Intercostals	21
Bulkheads	26
Diagonals	30
Cross Beam	33
IECM Shelf	35
Experiment Trays	37
TRAY EFFECTIVE PANEL STIFFNESS PROPERTIES	42
Stiffness Matrix From SPAR Tray Models.	42
Extrapolation of Rectangular End Tray Stiffness	49
Tray Panel Effective Properties	50
Extrapolation of Square End Tray Stiffness	53
STATIC TEST-ANALYSIS EVALUATION OF ATTACHMENTS	55
MASS PROPERTIES	57
COMPARISON OF FREQUENCIES AND MODE SHAPES	61
Configuration Without Trays	61
Configuration With Trays	61
REMARKS AND CONCLUSIONS	68
APPENDICES	69
A PANEL AND BEAM PROPERTIES	69

TABLE OF CONTENTS (CON'T)

	Page
B MESH SIZE CRITERION	75
C TRAY MASS MOMENTS OF INERTIA	78
D SPAR EIGENVALUE EXTRACTION EXPERIENCE .	83
REFERENCES	88

LIST OF FIGURES

Figure No.		Page
1	LDEF Structure Schematic	10
2	LDEF Dynamic Test Configuration With Trays	11
3	Forward End View of LDEF Without Trays	12
4	Side View of LDEF Without Trays	13
5	Longeron-Intercostal Joints and End Bulkhead	14
6	Interior Diagonal End Joint at Center Bulkhead	15
7	7.62 cm Side Experiment Tray Without Base Plate	16
8	Tray Structure Interface	17
9	LDEF SPAR Model	19
10	Longeron Grid Point Coordinates	22
11	Longerons and Intercostals	23
12	Longeron-Intercostal Attachments at Stations ± 4.4313 m.	24
13	Longeron-Intercostal Attachments at Stations ± 1.5304 m and ± 2.9401 m	25
14	Center Bulkhead at Station 0.0	27
15	Forward Bulkhead at Station -4.4313 m	28
16	Aft Bulkhead at Station 4.4313 m	29
17	Diagonals.	32
18	Cross Beam at Station -4.4313 m	34
19	IECM Shelf	36
20	Tray SPAR Model Used for Effective Panel Properties	38
21	Tray Locations and Total Weight	39
22	Extensional-Bending Coupling of a Shallow Side Tray	40
23	Shear-Twisting Coupling of the Deep Side Tray Base Plate	41
24	Analytical and Measured Static Deflections	56
25	LDEF SPAR and Test Vibration Modes Without Trays	62

LIST OF FIGURES (CON'T)

Figure No.		Page
26	First Lateral Bending Mode Without Trays	63
27	First Vertical Bending Mode Without Trays. . . .	64
28	First Torsion Mode SPAR	65
29	First Torsion Mode Test	66
30	Preliminary SPAR and Test Modes With Trays . .	67
31	Mesh Size Criterion	77
32	SPAR Eigensolutions for Free-Free Modes of LDEF	87

LIST OF TABLES

Table No.		Page
1	Substructure Groups	20
2	Displacement Boundary Conditions for Tray Static Models	48
3	Tray Panel Effective Orthotropic Properties. . . .	54
4	SPAR Grouping for Weight Balance, Configuration Without Trays.	58
5	Lumped Mass Locations, Confirguration With Trays .	59
6	SPAR Weight, Configuration With Trays	60
7	Flange Rotation Effect on 3 Inch Debris Panel Stiffness Matrix	71
8	Tray Panel Stiffness Terms.	72
9	SPAR Section Properties.	73
10	Summary of Side Tray Mass Offsets and Mass Moments of Inertia	81
11	Tray Mass Moments of Inertia Including Tray Ballast	82

SUMMARY

The purpose of this paper is to present the recent application of structural modeling of the Long Duration Exposure Facility (LDEF) utilizing the SPAR system of computer programs for vibration analysis.

The technical areas of interest consist of five parts:

1. Development of the LDEF finite element model.
2. Derivation of tray effective panel stiffness matrix using finite element tray models.
3. Assessment of attachment conditions and end fitting flexibility by comparing SPAR with test static displacements.
4. SPAR Grouping.
5. Derivation of the LDEF frequencies and mode shapes and comparing them with test.

Results indicate that the SPAR LDEF model gave good agreement between analytical and measured data. This was true for the frequencies of the LDEF model without trays and the LDEF model with trays. The static test data is valuable in assessing end fitting boundary conditions to be used in the finite element model.

INTRODUCTION

The Long Duration Exposure Facility (LDEF) vehicle will be launched in the space shuttle and placed in earth orbit with 86 trays, most of them containing passive experiments. After a period of time exposed to the space environment, LDEF will be retrieved by a second space shuttle flight, and its many experiments will be evaluated.

Because LDEF must interface with the space shuttle, it is important that the LDEF finite element dynamic model be an accurate representation of the actual structure. NASA Langley performed dynamic model survey testing and static testing of LDEF with and without the trays being installed. The SPAR finite element computer programs were used to model LDEF and the static test data was used for correlation and model improvement. SPAR has the advertized capability to perform a vibration analysis of a system with thousands of degrees-of-freedom (DOF) but the analyst must check every input to maintain the accuracy desired. The philosophy used in this LDEF-SPAR model was to keep the model as simple as possible but maintain the required accuracy and utilize a thorough checking of inputs. Each experiment tray was modeled as a single effective fully coupled six-by-six stiffness matrix panel. The stiffness matrix was obtained from static loadings on SPAR tray models. One of these tray models has 4356 DOF compared with 1416 DOF for the entire LDEF structure. Therefor, with 86 trays to model, the effective panel approach becomes most attractive.

The information in the body of this report presents the LDEF model construction, static test correlation for determining the joint boundary conditions and end fitting flexibility, how the tray effective panels were derived, and finally the comparison of frequencies and mode shapes with test data.

The information in the appendices consists of the panel and beam properties, the mesh size criterion, the tray moments of inertia, and the SPAR eigenvalue extraction experience.

SYMBOLS

General Notations

C_{ij}	Tray effective panel stiffness term - force in i direction due to a unit strain in j direction
d	distance between two panels
$d_x = \frac{M_x}{N_x}$	tray panel offset due to longitudinal extensional-bending coupling
$d_y = \frac{M_y}{N_y}$	tray panel offset due to lateral extensional-bending coupling
$d_{xy} = -\frac{M_{xy}}{N_{xy}}$	tray panel offset due to shear-twisting coupling
D	single panel bending stiffness
D'	effective panel bending stiffness
e_x, e_y	extensional strain
e_{xy}	shear strain
E	Young's Modulus
f	force
F	free boundary condition, applied load column matrix
$G = \frac{E}{2(1+\nu)}$	Shear modulus
h	thickness, height of circular arch at mid point
I	total tray plus ballast mass moment of inertia

I_b	tray ballast mass moment of inertia
I_t	tray mass moment of inertia
k	rotational strain
$k_x = -\frac{\partial^2 w}{\partial x^2}$	rotational strain in x direction
$k_y = -\frac{\partial^2 w}{\partial_x \partial_y}$	rotational strain in y direction
$k_{xy} = 2\frac{\partial^2 w}{\partial_x \partial_y}$	twisting strain
K	stiffness , stiffness matrix
K_r	stiffness of rigid element
L	length of effective tray panel
m	moment
M	bending stress resultant
M_{ij}	reaction moment at grid point i in the tray coordinate direction j
N	extensional stress resultant
P	applied static test load
P_{ij}	reaction force at grid point i in the tray coordinate direction j
r	rotation
R	static test reaction load

ss	simple support boundary condition
t	thickness
t_x	tray panel longitudinal effective thickness
t_y	tray panel lateral effective thickness
t_{xy}	tray panel shear effective thickness
u	extensional displacement
U	displacement column matrix
w	weight, deflection normal to surface
w_b	weight of tray ballast
W	width of effective tray panel
x, y, z	tray coordinate system
$\bar{z}_b$	tray ballast mass moment arm
$\bar{z}_t$	tray mass moment arm
α	percent displacement error by adding a rigid link in series with a flexible element
δ	deflection
θ	rotation displacement

ν	Poisson's Ratio
σ_i	stress in i direction
ω	angle of rotation between tray coordinate system, x,y,z, and the LDEF SPAR cylindrical coordinate system, r θ z'

SPAR Notations

ANG	angle section
BA	general beam elements
BB	beam 6 x 6 stiffness matrix
E21	general beam elements such as angles, tees, zees, tubes, etc.
E25	zero-length element used to elastically join two coincident grid points
E33	triangular membrane plus bending element
E43	quadrilateral membrane plus bending element
BRL	beam rigid link offset
CHN	channel section
GIVN	beam with extensional and bending stiffness specified
SA	shell section properties

TUBE	tube section
TEE	tee section
WFL	I section

Experiment Tray Notation

DP	7.62 cm (3 in) side Debris experiment tray
S	7.62 cm (3 in) side shallow tray
N	15.24 cm (6 in) side nominal tray
D	30.48 cm (12 in) side deep tray
SR	7.62 cm (3 in) end shallow rectangular tray
NR	15.24 cm (6 in) end nominal rectangular tray
DR	30.48 cm (12 in) end deep rectangular tray
SC	7.62 cm (3 in) end shallow square (corner) tray
NC	15.24 cm (6 in) end nominal square (corner) tray
DC	30.48 cm (12 in) end deep square (corner) tray
C_3	7.62 cm (3 in) rectangular end shallow tray stiffness
C_6	15.24 cm (6 in) rectangular end nominal tray stiffness
C_{12}	30.48 cm (12 in) rectangular end deep tray stiffness

LDEF STRUCTURAL TEST CONFIGURATION

The Long Duration Exposure Facility (LDEF) structure is primarily a bolted assembly of 6061 - T6 aluminum extrusions. The LDEF structure schematic is shown in Figure 1 indicating the principal dimensions and the design features for the 12 sided regular polygon. The polygon is 4.267 meters (14 feet) across the points and 9.144 meters (30 feet) long. The center and end bulkheads anchor the longerons and provide reaction points for the 8 diagonal tubes. The intercostals connected to the longerons divide the periphery into 72 equally sized rectangles. The center and end bulkheads are welded, the other joints are bolted. The center bulkhead has 2 trunnion fittings and a keel fitting that support the LDEF in the Shuttle bay. The forward bulkhead carries a trunnion fitting which acts thru a cross beam (Figure 3) to provide 2 other attachment points to the Shuttle. Figure 2 shows the aft end of the LDEF dynamic test configuration with the simulated trays installed. Figures 3 and 4 show the forward end and the right side respectively of the LDEF structure without trays in the transportation vehicle.

The longeron-intercostal joint design is identified in Figure 5 by the triangular arrows. These are pin-clevis joints at each end of the intercostals as shown in Figures 12 and 13. The clevis bolts are in the LDEF longitudinal direction and can be considered as pinned joints in a finite element model. However, the clevis tolerance is such that some relative rotational motion could occur about the 2 mutually perpendicular axes normal to the bolt axis. Therefor, the analysis considered both pinned and ball joints at these connections.

The eight diagonal tubes can best be seen in Figure 4 with the detail of the end joint at the center bulkhead shown in Figure 6. These clevis type pin joints are in reality ball joints because of their internal design. Two ball joints connect to a common flat plate type fitting extending from the center bulkhead. The original SPAR model considered this flat plate fitting as a rigid link while a later refinement included its flexibility.

The LDEF side trays are riveted 6061 - T6 aluminum alloy angle and sheet of either 0.160 cm (.063 in) or 0.3175 cm (0.125 in) thickness with 0.3175 cm (.125 in) T or I section bottom cross beam members. Both the T and I sections can be seen in Figure 7. The side tray experiment envelope is approximately 1.219 m long and 0.914 m wide with depths of 7.62, 15.24 and 30.48 cm (3, 6

and 12 in). The end tray envelope is approximately .762 m square with depths of 7.62, 15.24 and 30.48 cm (3, 6 and 12 in). Figure 7 shows a 7.62 cm (3 in) side shallow tray mounted on a longeron-intercostal frame. The base plate of the experiments are bolted to the bottom framework at some of the many nut plate locations provided. For the LDEF dynamic configuration, all of the experiments except the Debris tray were represented by a single 0.457 cm (0.18 in) aluminum base plate with 1, 2 or 3 stacks of aluminum ballast plates to represent the correct experiment mass. Each ballast stack was bolted to the base plate at the four corners of the stack. These bolts can be seen in Figure 2 and 6. The Debris tray consists of two 0.457cm (0.18 in) aluminum plates with no ballast plates, with each plate covering one half of the tray bottom. Each Debris plate was bolted to the tray bottom frame with 15 bolts. All of the other trays with a single base plate were bolted to the tray bottom with 6 bolts, 4 at the corners and 2 to the center framework. Figures 7 and 8 show the tray structure interface for a side tray. There are no bolts passing through the tray lip. The tray clamp design allows the tray to expand in the plane of the tray, due to thermally induced loads, by overcoming the clamp friction load. For the dynamic analysis the four corner clamps were considered to have no relative motion between the tray lip and the LDEF structure. The four side clamps were assumed to allow relative rotation about an axis normal to the tray lip.

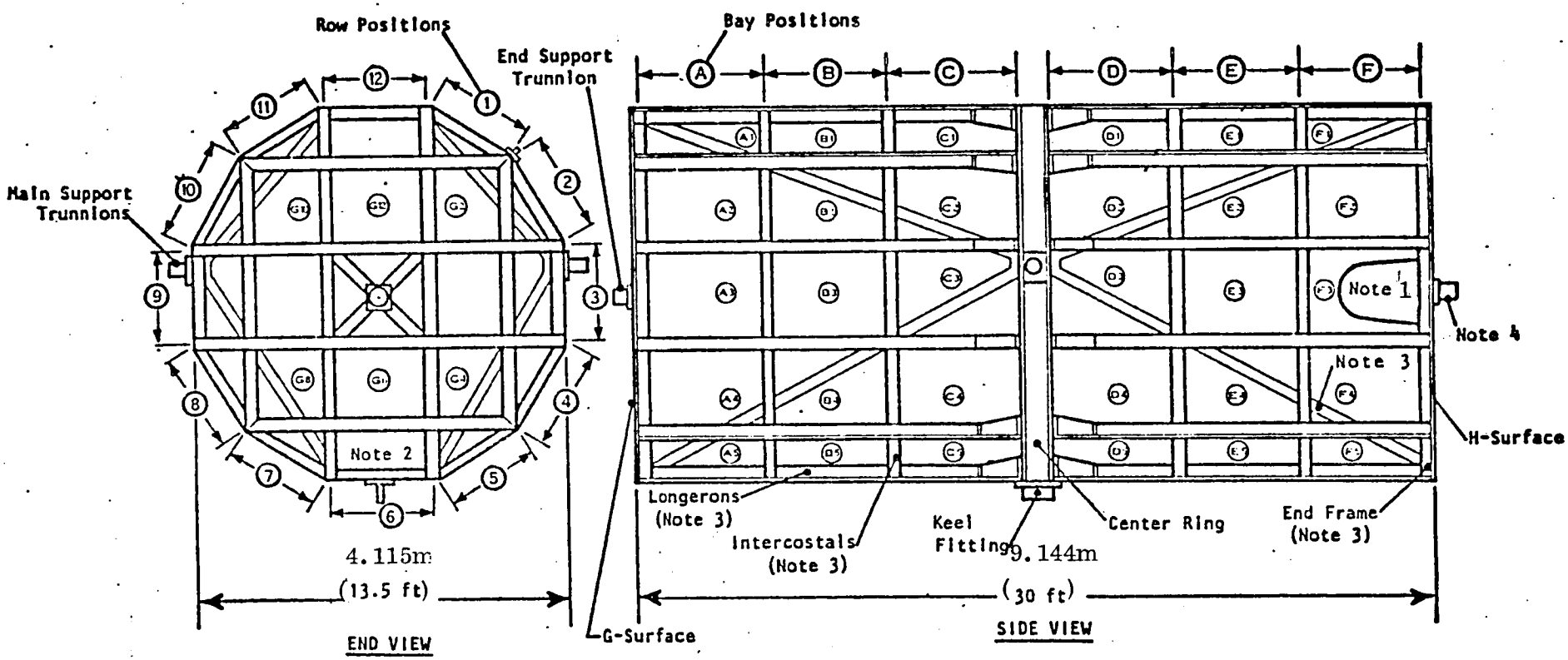

Note:

1. Location for a Magnetic Viscous Damper.
2. All openings on the LDEF are covered by either a tray or plate.
3. Longerons - 17.78 cm (7 in) Aluminum I-Section, End Frames - 15.24 cm (6 in) Aluminum I-Section, Diagonals - 15.24 cm (6 in) Aluminum Tube. Intercostals are Aluminum T-Sections, one half of a 17.78 cm (7 in) I-Section.
4. Auxiliary Trunnion for Ground Handling Only. Removed before flight.

Figure 1. LDEF Structure Schematic

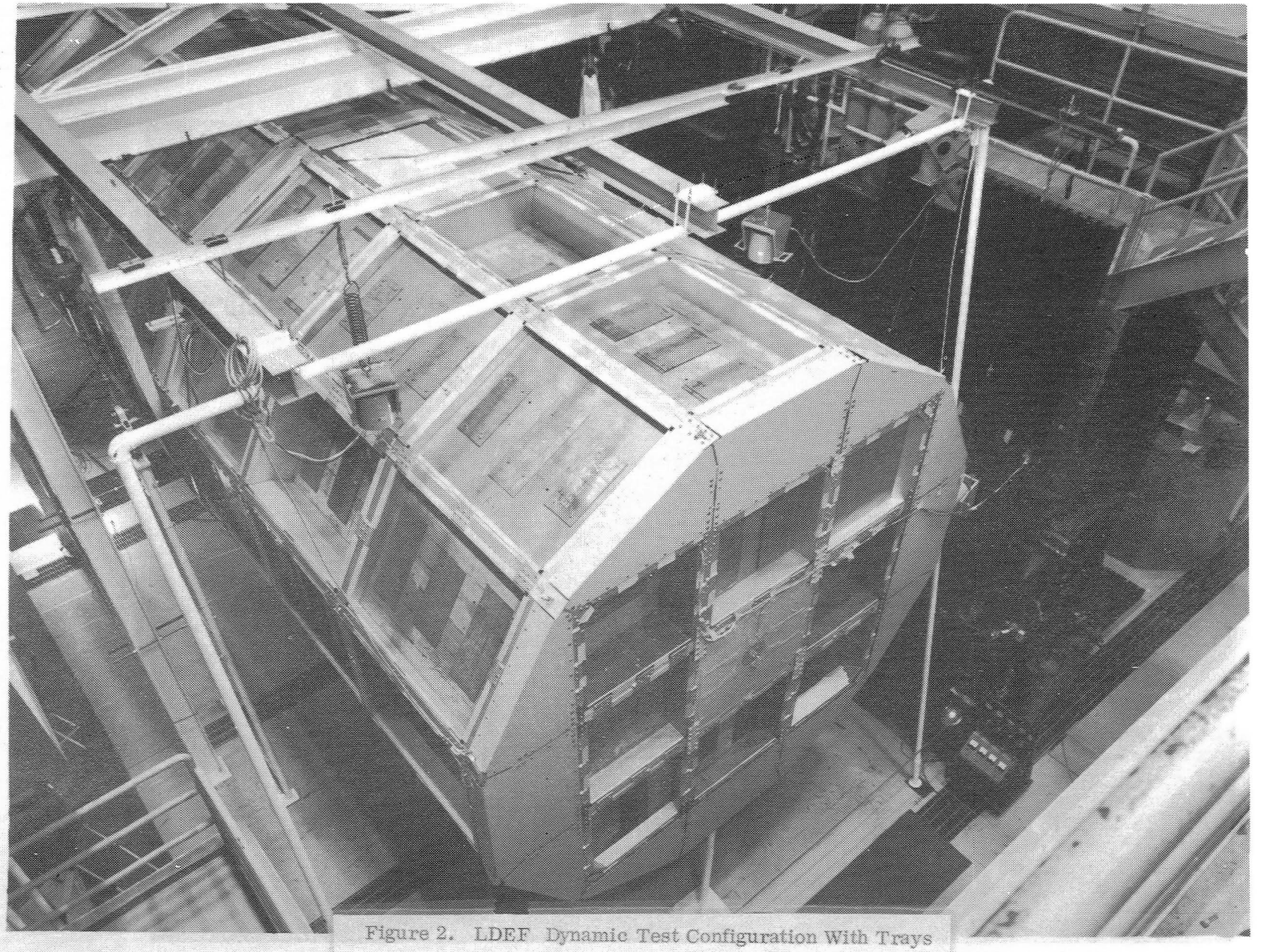

Figure 2. LDEF Dynamic Test Configuration With Trays

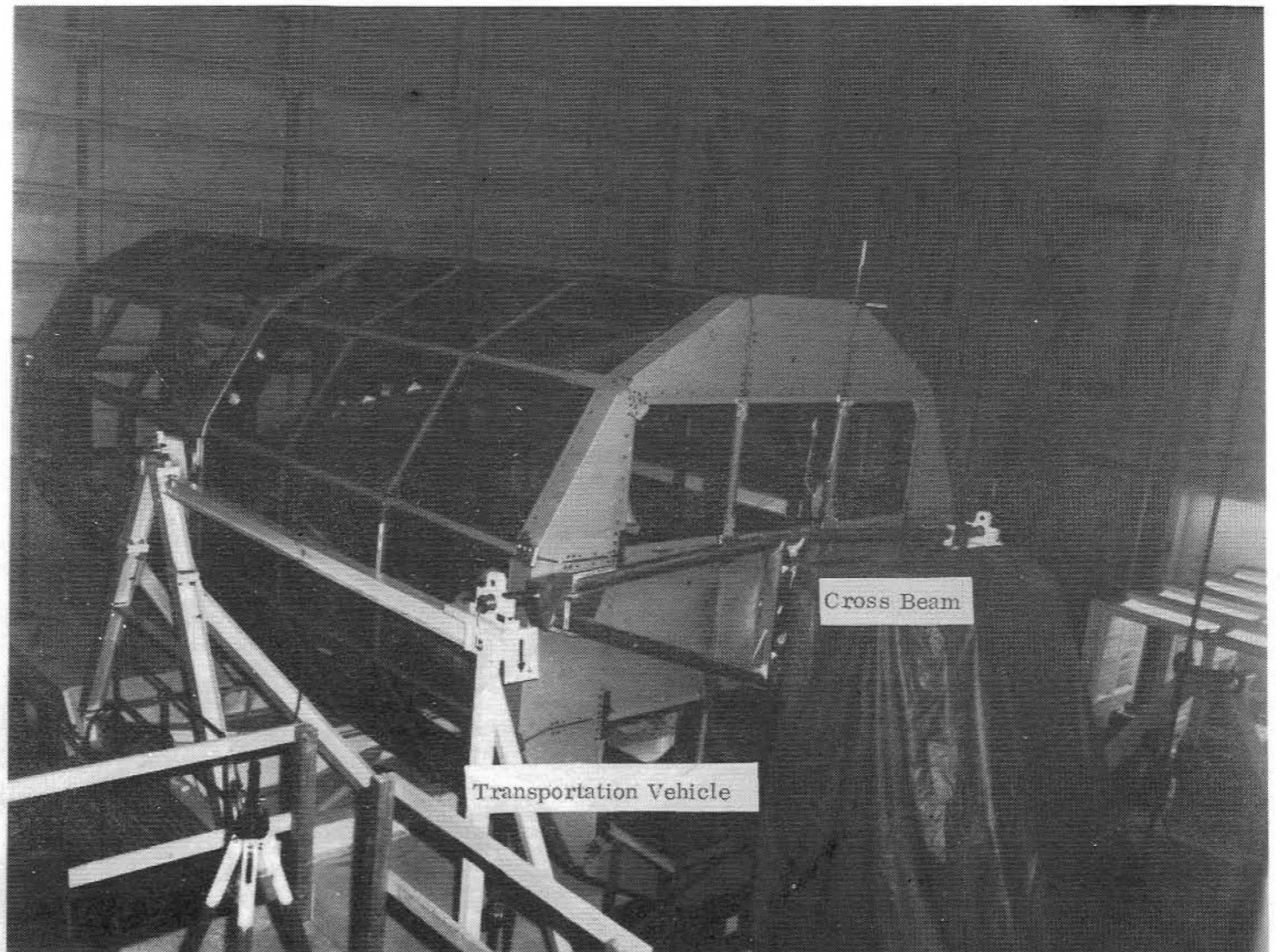

Figure 3. Forward End View of LDEF Without Trays

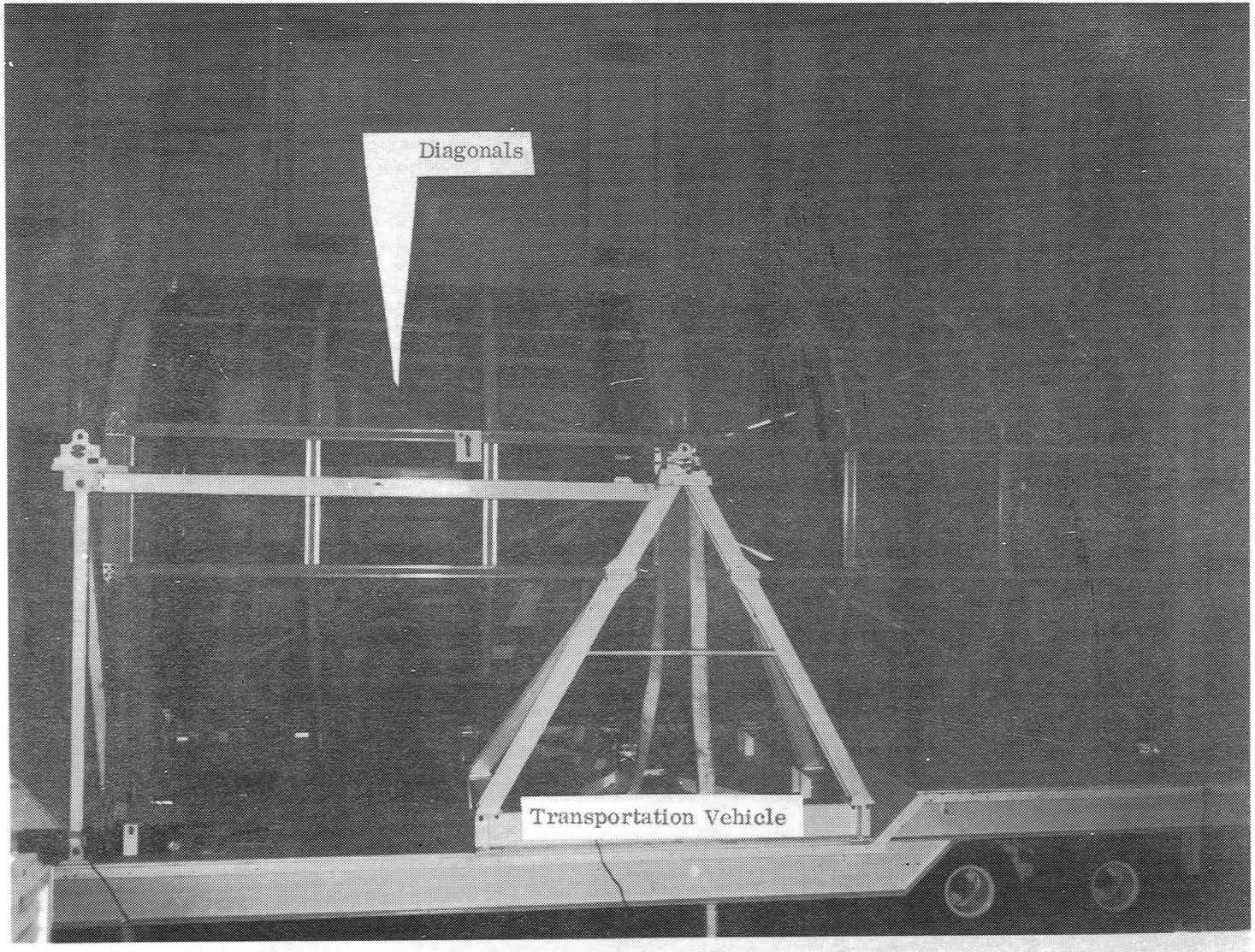

Figure 4. Side View of LDEF Without Trays

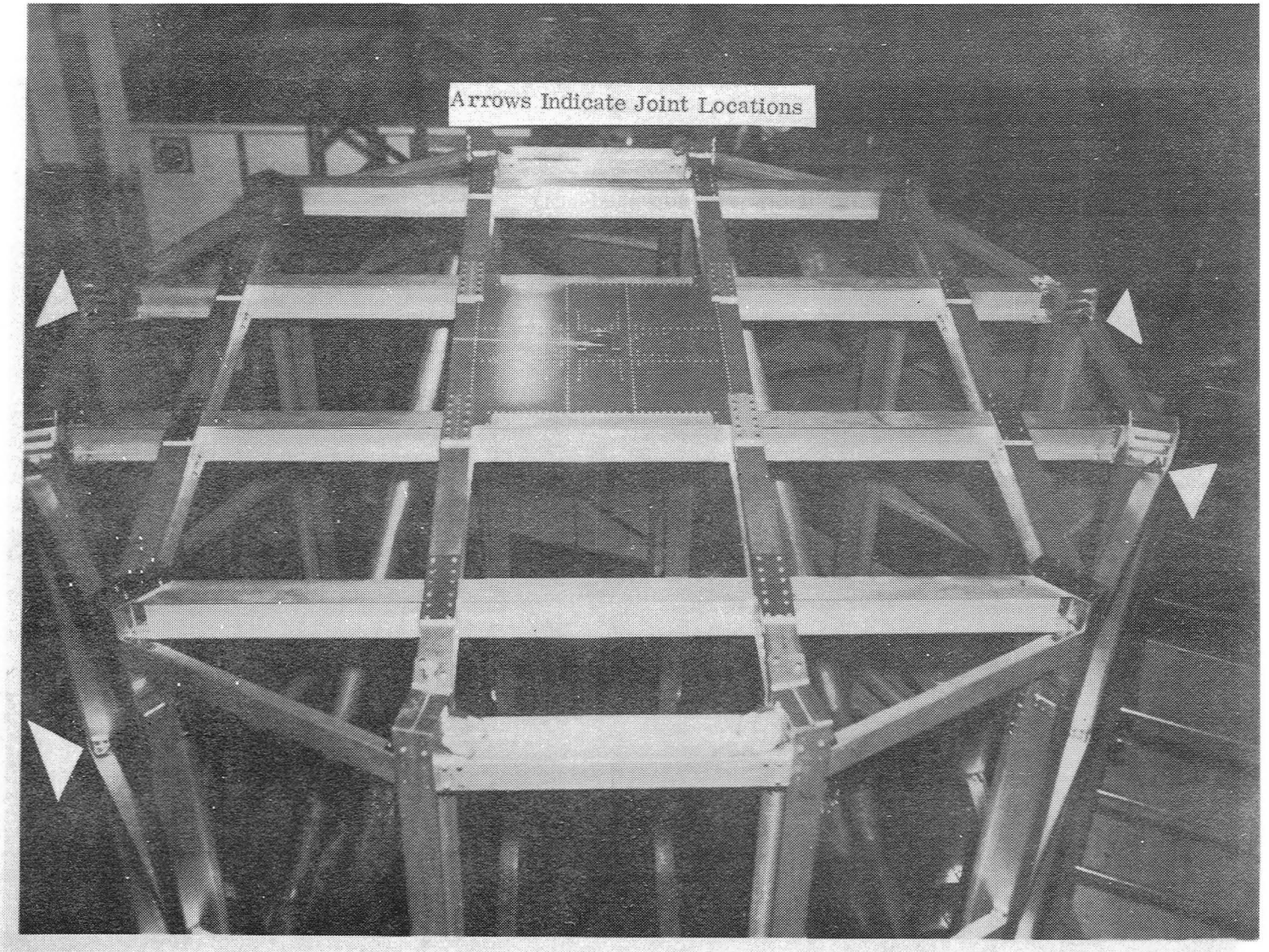

Figure 5. Longeron-Intercostal Joints and End Bulkhead

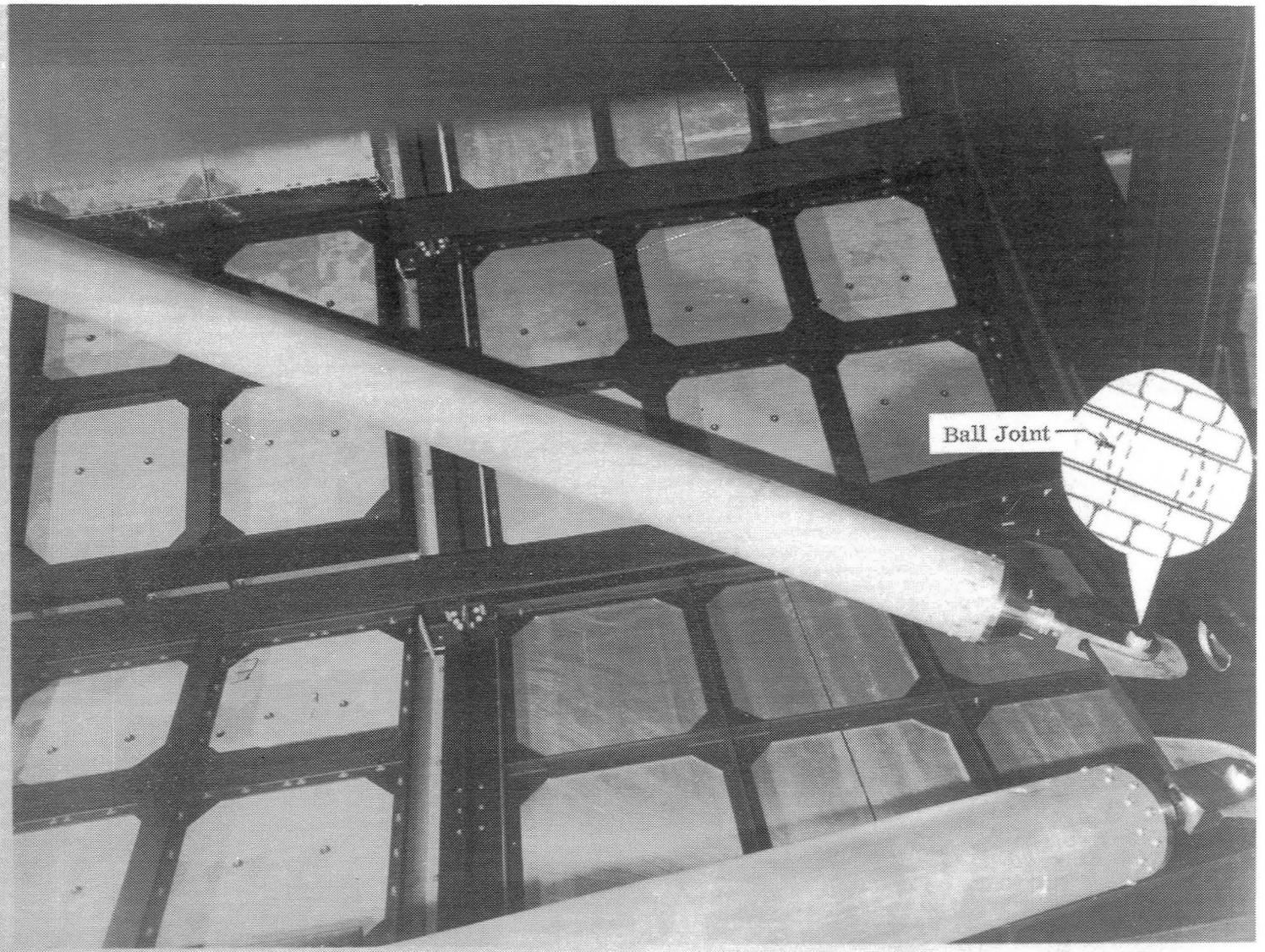

Figure 6. Interior Diagonal End Joint at Center Bulkhead

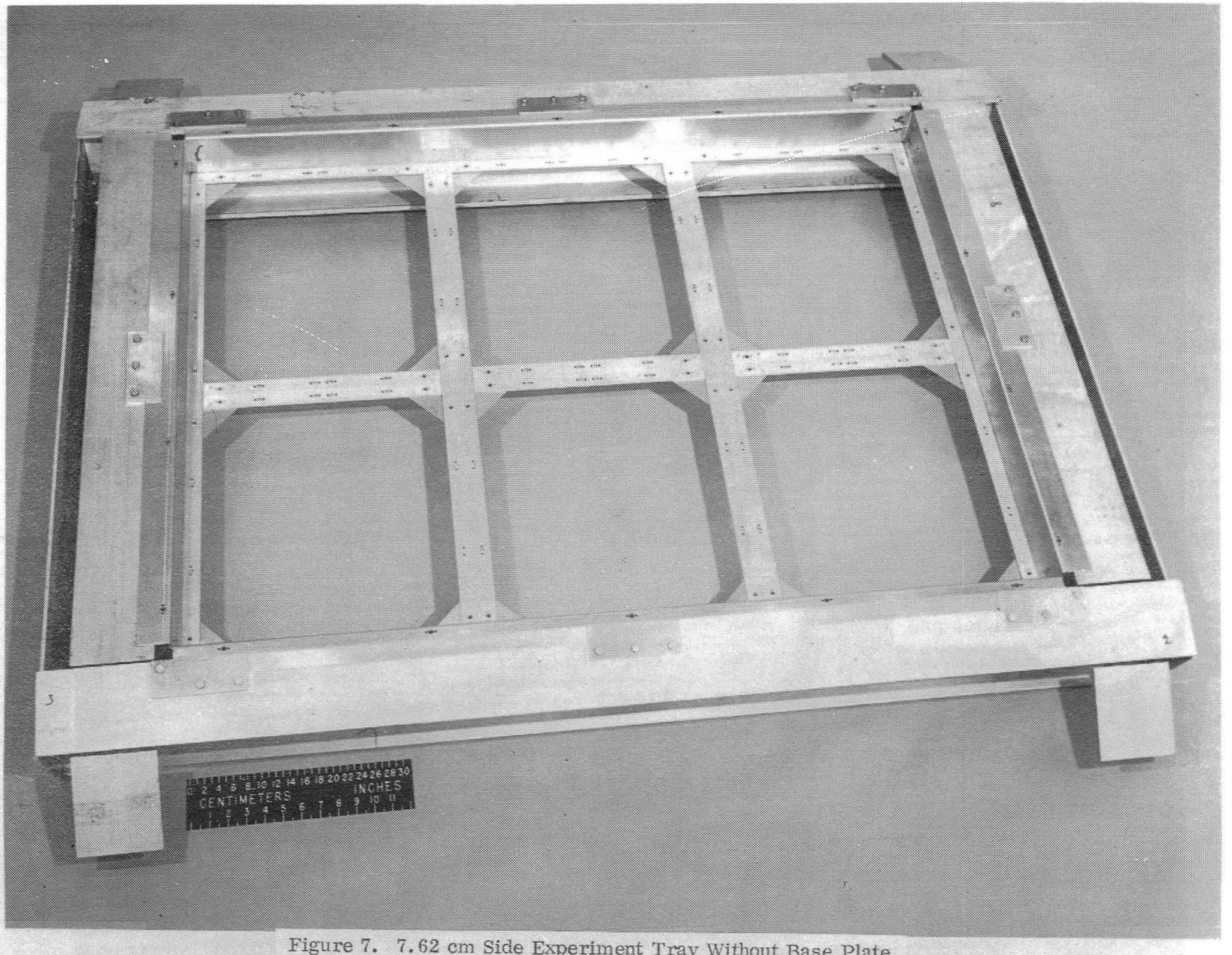

Figure 7. 7.62 cm Side Experiment Tray Without Base Plate

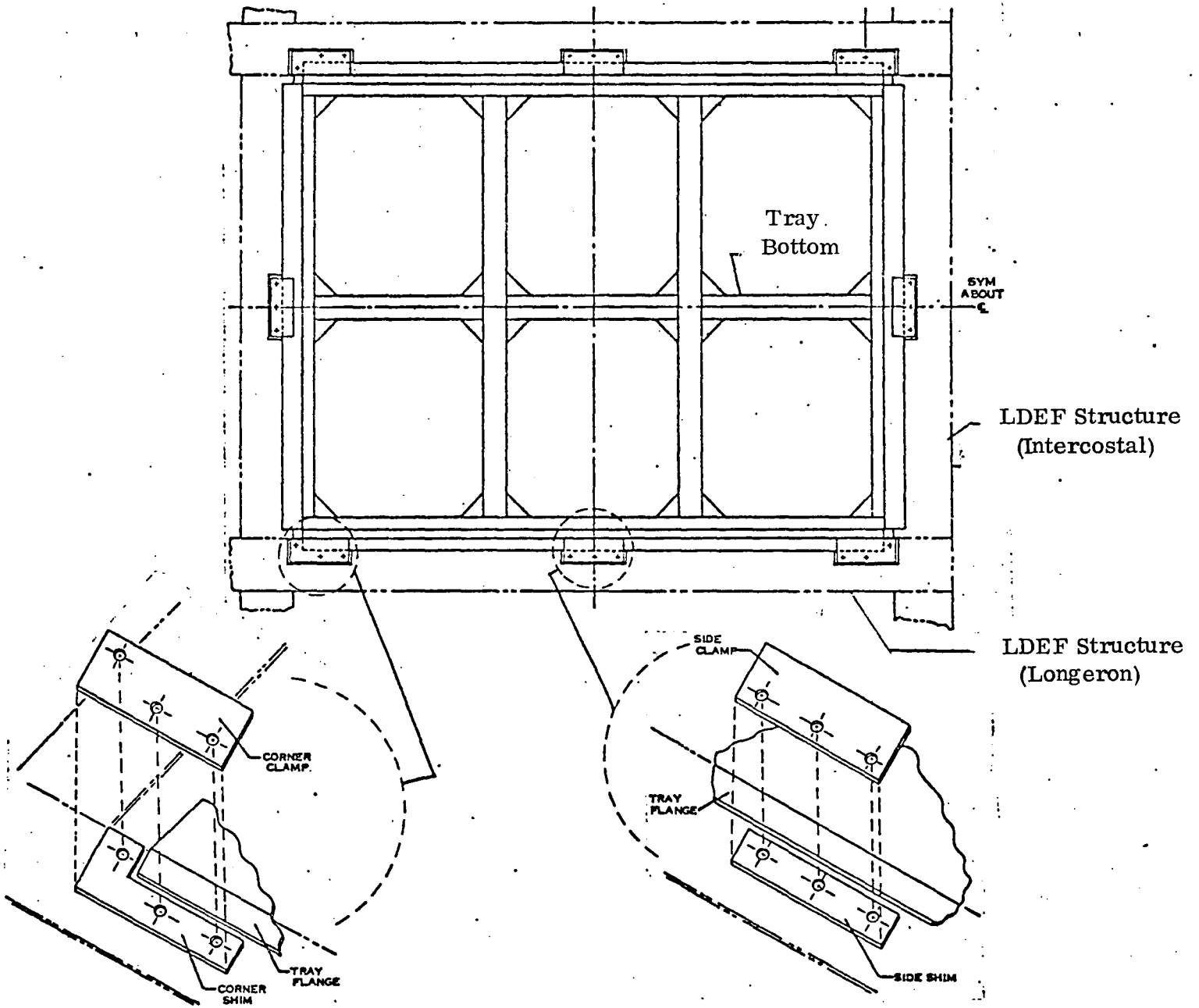

Figure 8. Tray Structure Interface

SPAR LDEF MODEL

The SPAR computer programs of Reference 1 were used for the LDEF finite element modeling and for the subsequent static and dynamic analysis. Figure 9 shows a computer print out of the undeformed shape of the SPAR model. The bottom, side and end views are shown. The model has 236 grid points with 1416 degrees of freedom. There are 381 beam elements, 16 three node elements and 92 four node elements. The circles in Figure 9 represent the 16 ball joints at the ends of the 8 diagonals. The model shown is the final configuration that includes the diagonal end flexibility of the flat plate fittings between the center bulkhead and the ball joints. The original model had rigid links for these flat plate fittings. The triangle represents a pin joint that allows the cross beam to rotate about the 3 axis relative to LDEF. The dots show the longeron-to-intercostal joint locations that were treated as pin or ball joints in the analysis. In most cases each dot represents two pin joints as shown in Figures 12 and 13 so that the 12 grid points per station results in 24 pin joints per station. However, at the forward and aft bulkheads,the top and bottom intercostals are of different construction and do not have clevis pin joints as shown in Figure 5. There are still 12 grid point locations but only 20 pin or ball joints per station making a total of 136 of these joints in the LDEF model. There are no pin or ball joints at the center bulkhead.

SPAR has the capability of subdividing the model into groups of substructure elements. This grouping has the advantage of visually checking each group plot for modeling errors and obtaining the weights of each group for comparison with actual weights for weight distribution control. The SPAR model was divided into the substructure groups shown in Table 1.

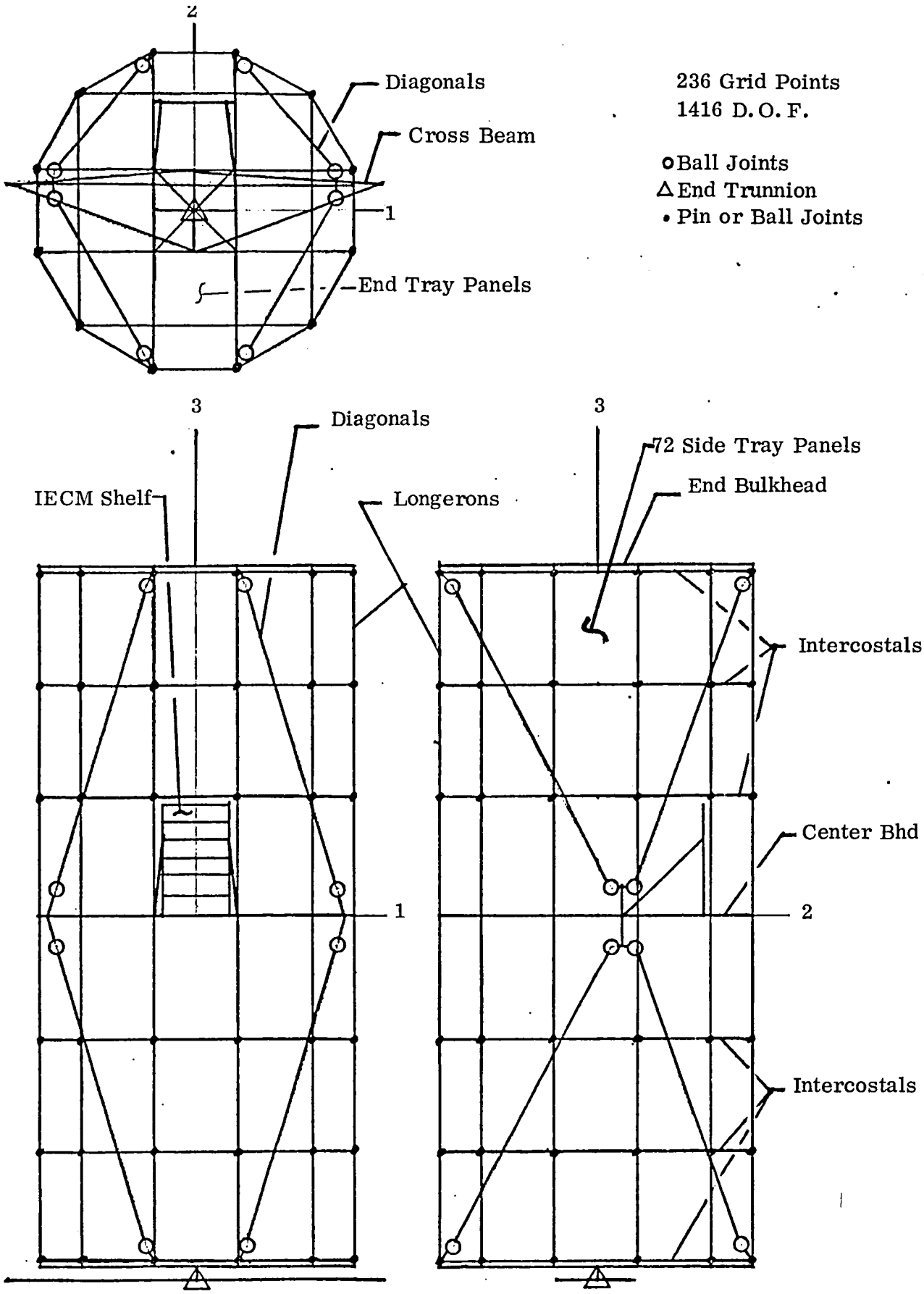

Figure 9. LDEF SPAR Model

TABLE 1. SUBSTRUCTURE GROUPS

Modeling Sequence	SPAR Group	Element Type	No. of Ele.	Figure
1 Longerons	E21-1	Beam	96	10
2 Intercostals	E21-2	Beam	72	11
3 Center BHD	E21-3	Beam	30	14
4 Forward BHD	E21-4	Beam	40	15
	E33-1	Triangular Plate	8	
5 Aft BHD	E21-5	Beam	40	16
	E33-2	Triangular Plate	8	
6 Diagonals	E21-6	Beam (Tube)	32	17
	E25-2	Zero length beam (ball joints)	16	9
	E21-9	Beam (end attach.)	20	17
7 Cross Beam	E21-7	Beam	13	18
	E25-1	Zero length beam (pin joint)	1	9
8 IECM Shelf	E21-8	Beam	21	19
	E43-1	Quadrilateral Plate	6	
9 Exp. Trays				
Debris Side	E43-2	Quadrilateral Plate	22	
Shallow Side	E43-3	Quadrilateral Plate	26	
Nominal Side	E43-4	Quadrilateral Plate	14	
Deep Side	E43-5	Quadrilateral Plate	10	
End-Rectangular	E43-6	Quadrilateral Plate	6	
End-Corner	E43-7	Quadrilateral Plate	8	

Longerons and Intercostals

The first substructure group modeled was the longeron group. The longerons consist of 12 forward and 12 aft I beams attached to the center bulkhead. Each longeron, at location A through L in Figure 10, was divided into four beam elements as shown at the intercostal attachment points resulting in a total of 96 beam elements. Figure 11 identifies all of the longeron grid point numbers and the SPAR section property used. The second substructure group modeled consisted of the 72 intercostals tabulated in Figure 11. Figures 12 and 13 show the actual longeron to intercostal attachment and the SPAR model configuration. The longeron beam elements were connected to grid points located on the longeron neutral axis. The intersection of the neutral axes of two adjacent intercostals fell outboard of the longeron neutral axis as shown in Figure 12. The intercostal beam elements were modeled with beam rigid link offsets (BRL) to locate the intercostal beam elements at their neutral axes. To avoid adding two additional grid points attached by a zero length beam elements for each pin joint, the intercostal beam elements bending stiffness was set equal to zero to simulate the pin ended condition. For a ball-joint end conditions both of the bending and the torsional stiffnesses of the beam elements were set equal to zero. The SPAR section property BA16 was used for the ball-joint end condition and BA18 was used for the pin-joint end condition. Both of these section properties have some of the tee section properties(BA2) set equal to zero as shown in Appendix A (Table 9).

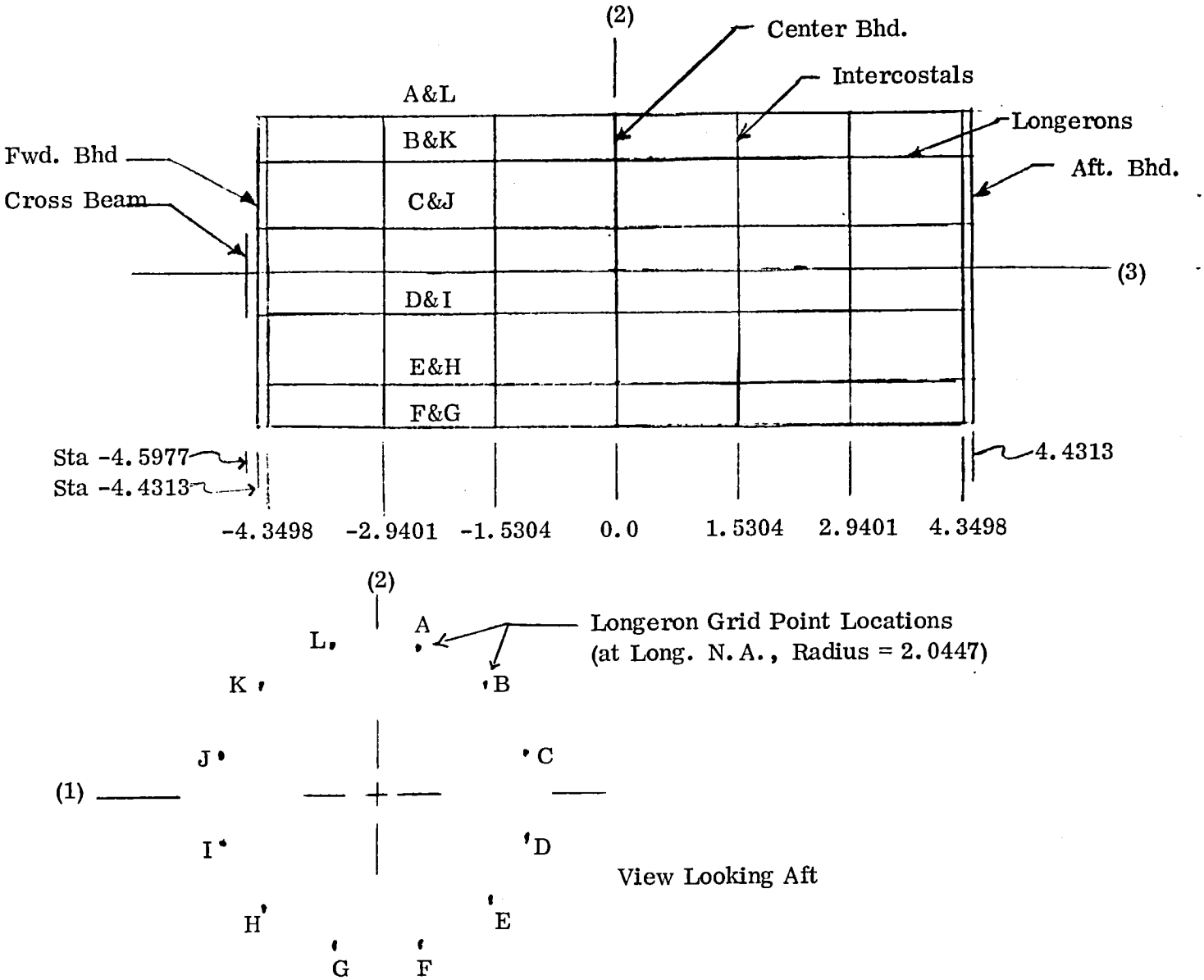

Location	Coordinates (1)	(2)
A	-.529206	1.975028
B	-1.445821	1.445821
C	-1.975028	.529206
D	-1.975028	.529206
E	-1.445821	-1.445821
F	-.529206	-1.975028
G	.529206	-1.975028
H	1.445821	-1.445821
I	1.975028	-.529206
J	1.975028	.529206
K	1.445821	1.445821
L	.529206	1.975028

Figure 10. Longeron Grid Point Coordinates (All Dimensions in Meters)

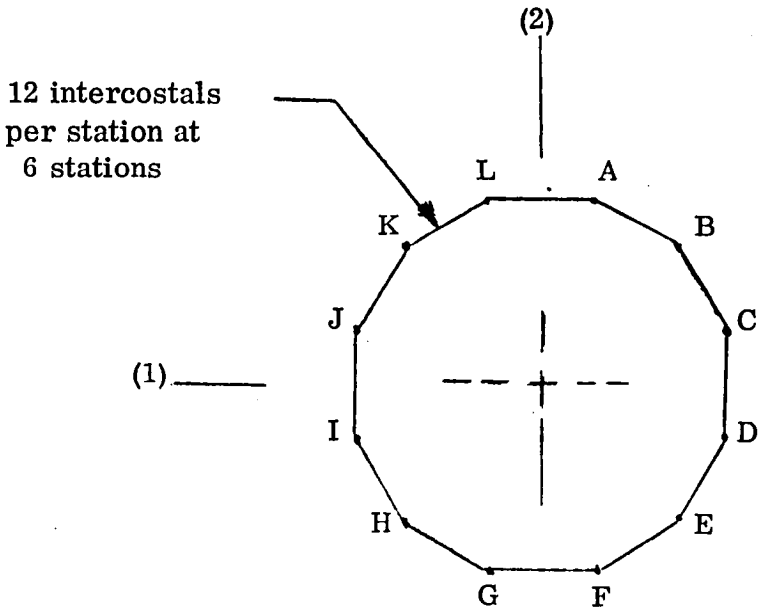

Type of Structure	Station (m)	Longeron Location (See Figure 10)											
		A	B	C	D	E	F	G	H	I	J	K	L
		Grid Point Numbers											
Fwd Bhd.	-4.4313	10	11	12	13	14	15	16	17	18	19	20	21
Intercos.	-4.3498	35	36	37	38	39	40	41	42	43	44	45	46
Intercos.	-2.9401	47	48	49	50	51	52	53	54	55	56	57	58
Intercos.	-1.5304	59	60	61	62	63	64	65	66	67	68	69	70
Center Bhd.	0.0	71	72	73	74	75	76	77	78	79	80	81	82
Intercos.	1.5304	113	114	115	116	117	118	119	120	121	122	123	124
Intercos.	2.9401	125	126	127	128	129	130	131	132	133	134	135	136
Intercos.	4.3498	137	138	139	140	141	142	143	144	145	146	147	148
Aft. Bhd.	4.4313	149	150	151	152	153	154	155	156	157	158	159	160

SPAR Section Property (Table 9)	No. of Elements	
BA1	96	17.78 cm (7. in) I beam - all longerons
BA1	4	top and bottom intercostals at end stations
BA16	68	Ball Joint } 8.89 cm (3.5 in) T section (BA2) - all other intercostals
or		
BA18	68	Pin Joint }

Figure 11. Longerons and Intercostals

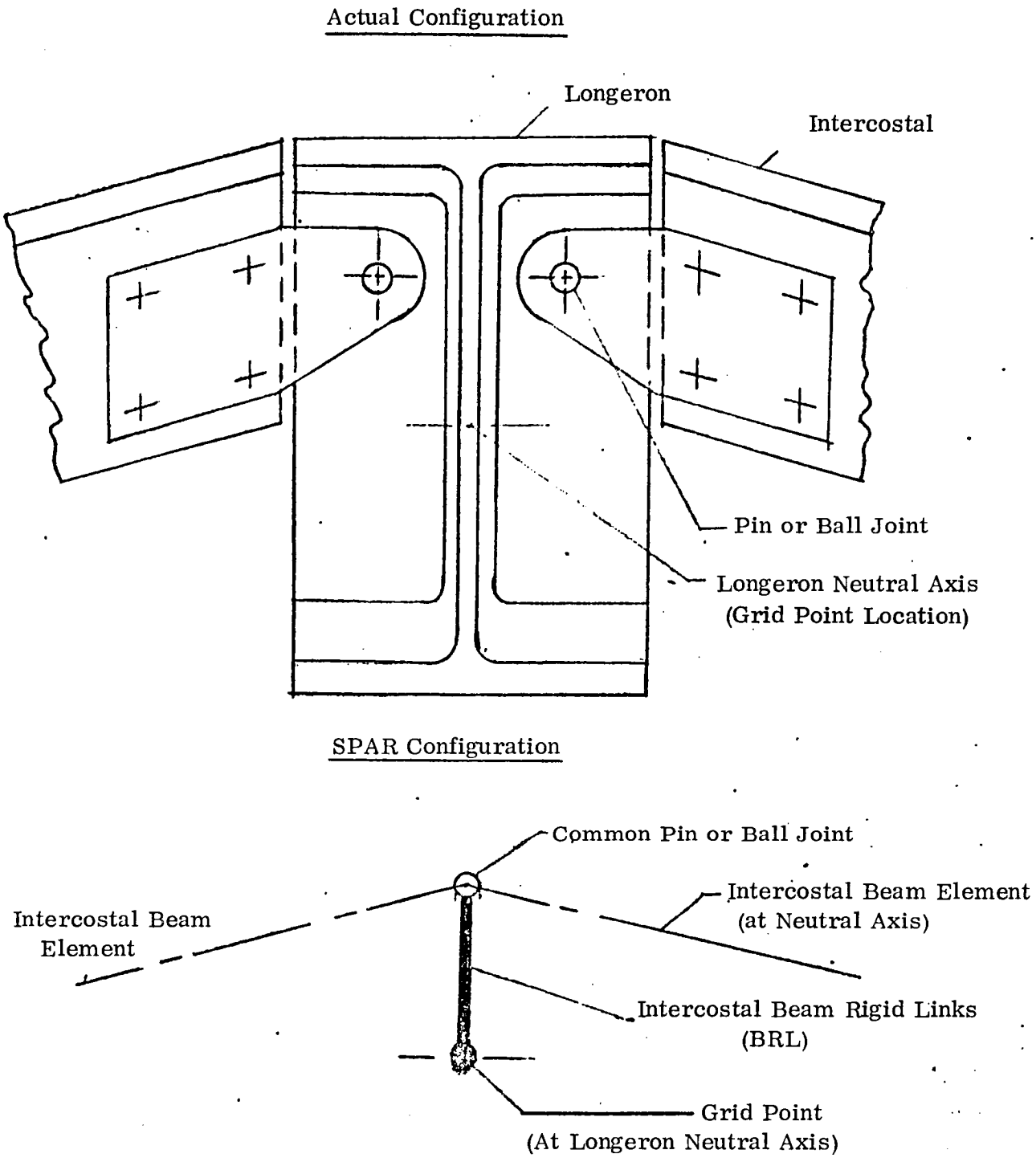

Figure 12. Longeron-Intercostal Attachments at Stations ± 4.4313m

Actual Configuration

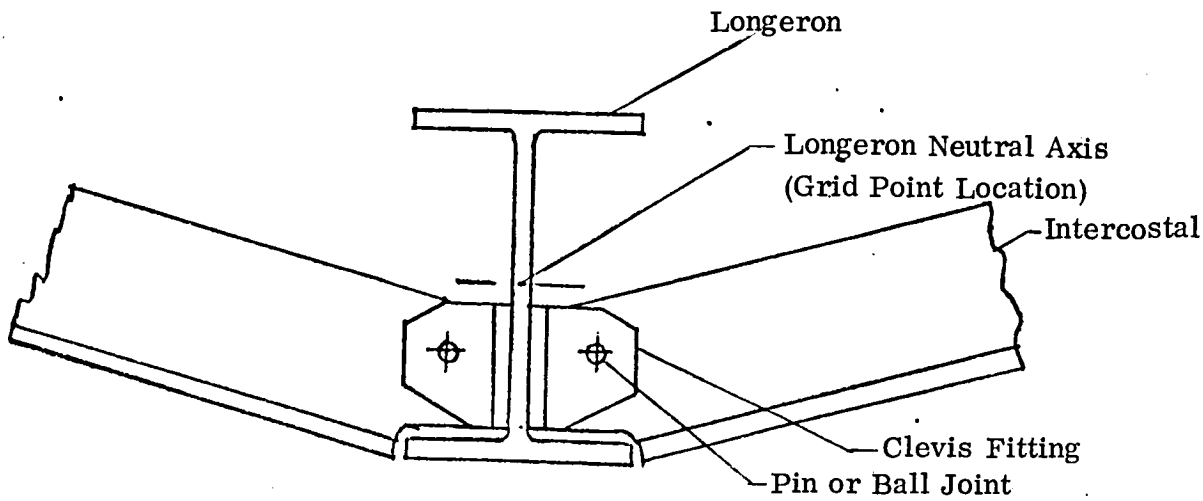

SPAR configuration similar to Figure 12.

Figure 13. Longeron Intercostal Attachments at Stations ± 1.5304m and ± 2.9401m

Bulkheads

The third substructural group modeled was the center bulkhead made up of 30 beam elements as shown in Figure 14. There are 14 vertical and lateral I beam members with the outer 14 ring elements representing a box section made up of two channel sections with inner and outer webs attached. Grid points 71 through 82 are the longeron grid points. Grid points 83 and 88 are the locations of the main support trunnion fittings and grid points 84 and 87 the attachment points for the 8 diagonals. Grid points 99 and 100 are the attachment points for each side of the IECM shelf. All beams are located at their neutral axes and beam rigid link offsets were used to join the beam element ends. The fourth and the fifth substructure groups are the identical forward and aft bulkheads shown in Figures 15 and 16. They each have 40 beam elements and 8 triangular plate elements. Grid points 10 through 21 and 149 through 160 are the longeron grid points. Grid point 28 connects to the cross beam. All of the vertical and horizontal beam elements represent I beam sections except the four connected to the center grid points. These four beams are box sections made up of two channel sections opening outboard with plates on the forward and aft surfaces. The eight triangle plate elements represent two plates 15.24 cm (6 in) apart. These two plates were input as a single effective panel stiffness matrix by using the FORMAT = 2 option in shell section properties (SA) inputs. The derivation of these properties is shown in Appendix A. The two plates are assumed to bend as a single panel and have an extentional stiffness equal to the sum of the two plates. The effective panel bending stiffness is:

$$D' = \frac{Et}{(1 - \nu^2)} \left(\frac{1}{2} d^2 + dt + \frac{2}{3} t^2 \right) \qquad (1)$$

where

$t = .3556$ cm (.14 in)

$d = 15.24$ cm (6. in)

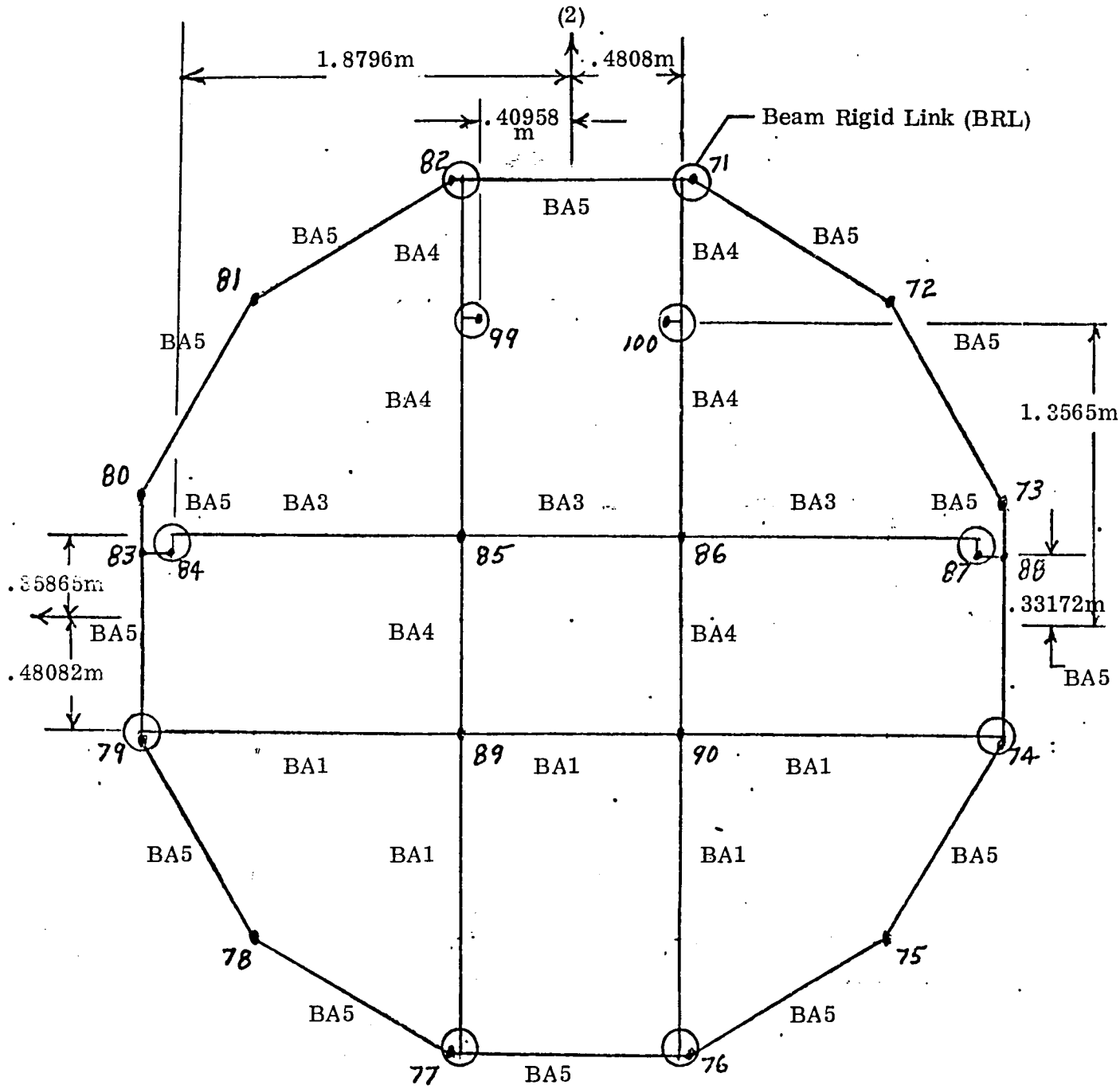

SPAR Section Property (Table 9)	No. of Elements
BA1	5 - 17.78 cm (7 in) I beam
BA3	3 - 30.48 cm (12 in) I beam
BA4	6 - 24.13 cm (9.5 in) I beam (average section)
BA5	16 - Built up Box Section

Figure 14. Center Bulkhead at Station 0.0

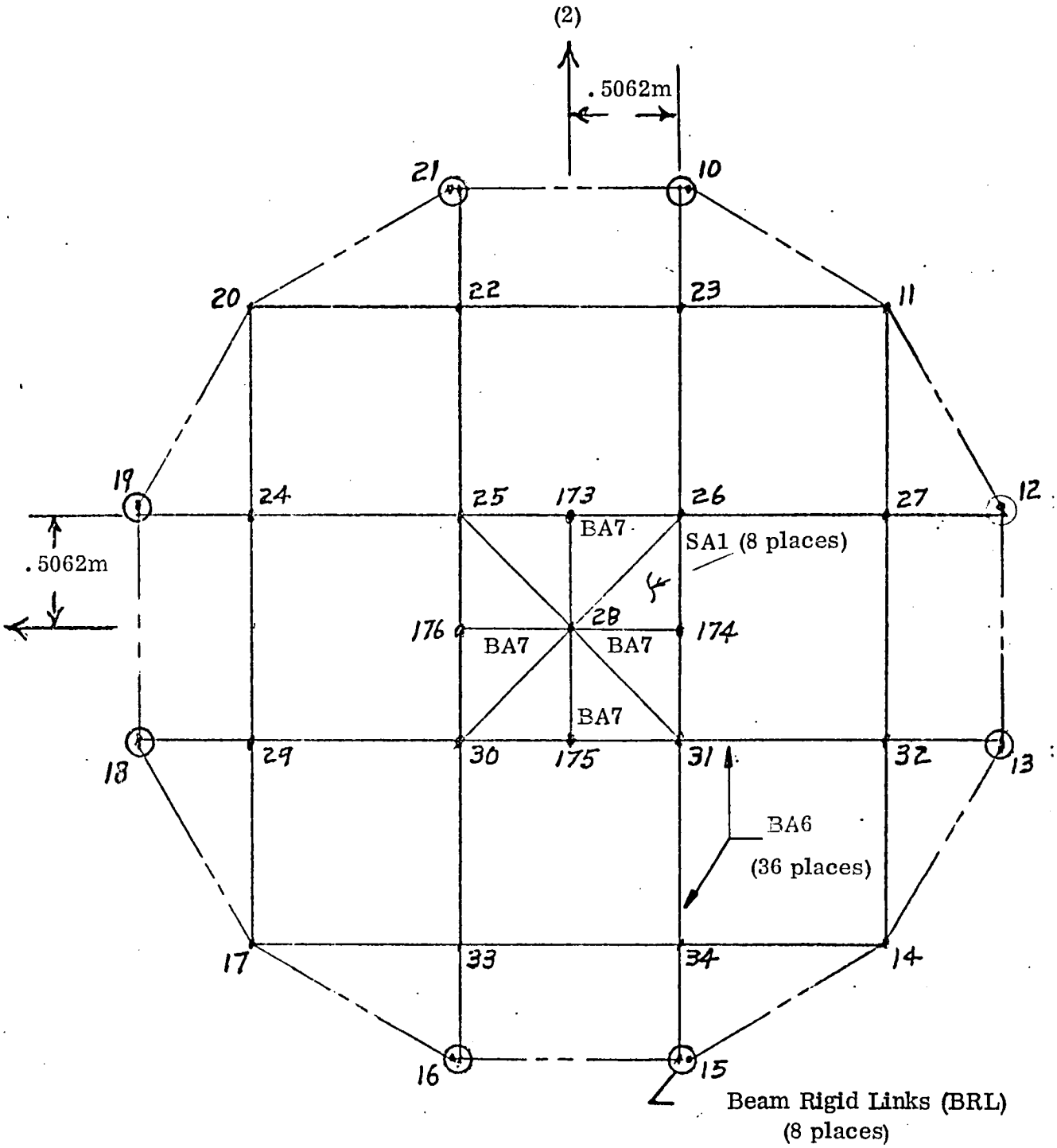

SPAR Section Property (Table 9)	No. of Elements
BA6	36 - 15.25 cm (6 in) I beams
BA7	4 - 35.56 x 25.4 cm (14. x 10. in) built up box beams
SA1	8 - Triangular panel elements

Figure 15. Forward Bulkhead at Station - 4.4313m

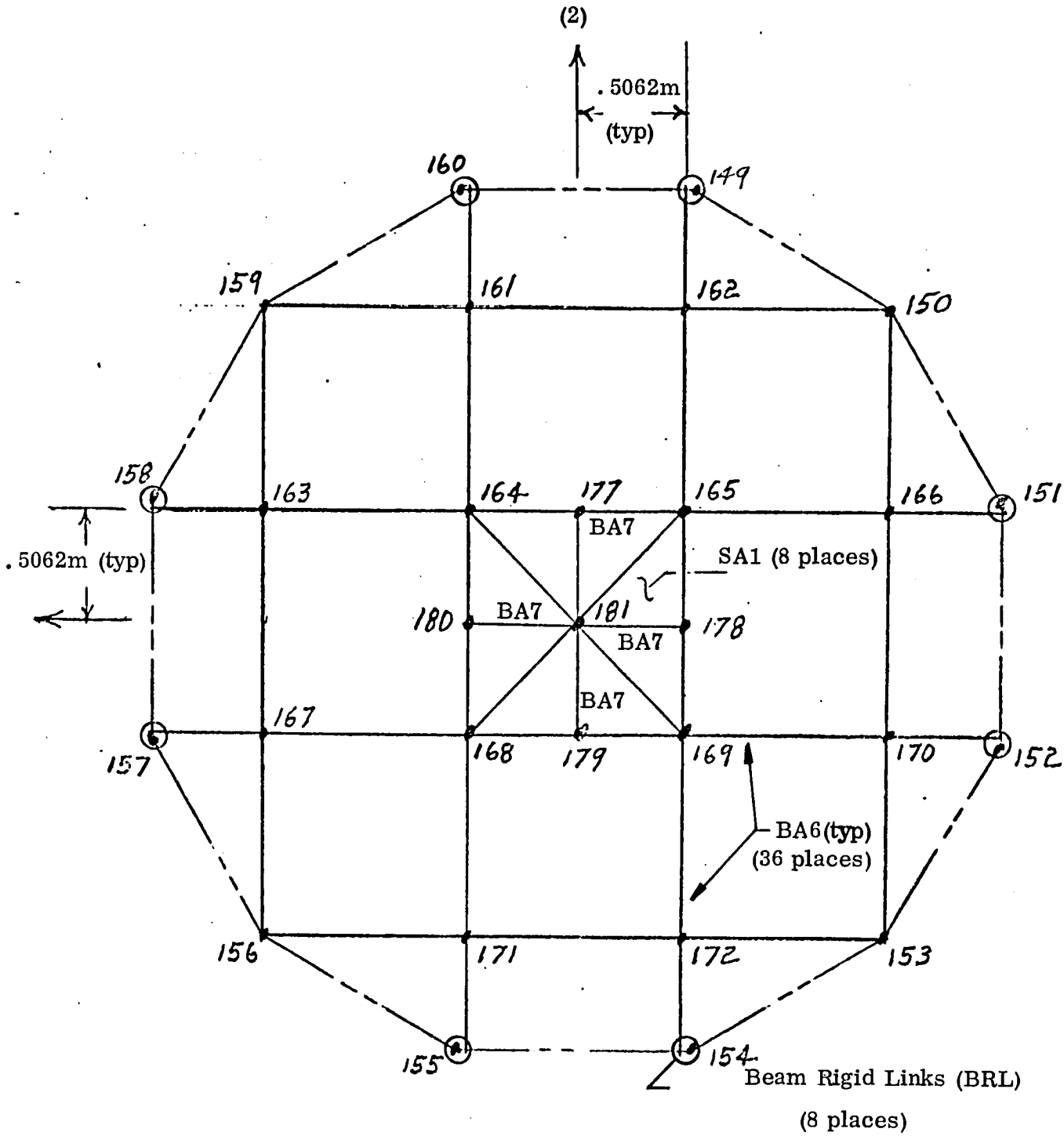

SPAR Section Property (Table 9)	No. of Elements
BA6	36 - 15.25 cm (6 in) I beams
BA7	4 - 36.56 x 25.4 cm (14 x 10. in) built up box beams
SA1	8 - Triangular panel elements

Figure 16. Aft Bulkhead at Station 4.4313 m

Diagonals

The sixth substructure group modeled was that of the eight diagonal tubes with the end ball joints and end attachment fittings shown in Figure 17. The circles represent the 16 ball joints. Flexible beam elements connect the ball joints to grid points 84 and 87 on the center bulkhead and at eight grid points on the longerons near the end bulkheads. The original model had rigid links from the ball joints to these end grid points. The ball joints were modeled by locating two grid points at the ball joint location and connecting them with a zero length element (E25) using a beam six-by-six intrinsic stiffness matrix input (BB) in SPAR. The stiffness matrix, K , is defined as

$$F = KU \tag{2}$$

where

$$F = (f_1\ f_2\ f_3\ m_1\ m_2\ m_3)^T$$

$$U = (u_1\ u_2\ u_3\ r_1\ r_2\ r_3)^T$$

In the above f, m , u and r equal applied force, applied moment, displacement and rotation at the origin of the beam element in the global coordinate system. For the diagonal ball joints, the K matrix takes the form

$$K = \begin{bmatrix} K_{11} & 0 & 0 & 0 & 0 & 0 \\ 0 & K_{22} & 0 & 0 & 0 & 0 \\ 0 & 0 & K_{33} & 0 & 0 & 0 \\ 0 & 0 & 0 & 0 & 0 & 0 \\ 0 & 0 & 0 & 0 & 0 & 0 \\ 0 & 0 & 0 & 0 & 0 & 0 \end{bmatrix} \tag{3}$$

The diagonal term is set equal to zero for each unrestrained degree of freedom desired. The diagonal terms not set equal to zero represent the "rigid spring" (K_r) that is in series with the flexible element. The value must be large enough to limit the displacement error but not so large as to result in computer computational errors. The "rigid link stiffness," K_r, required to obtain a given displacement error (α) was obtained from:

$$\alpha = \frac{100K}{K_r} \tag{4}$$

where

α — The percent displacement error of a "rigid" element (K_r) in series with a flexible element (K) compared with the displacement of K by itself.

For the diagonal elements, the extensional stiffness, K, of the upper diagonal was 48.6906 MN/m (.27803 x 10^6 lb/in). The value of 700508 MN/m (4.0 x 10^9 lb/in) was used for K_r indicating a diagonal extensional error of 0.007 percent. This value of K_r was used for K_{11}, K_{22} and K_{33} in equation (3).

Each tube was divided into four equal beam elements. The mesh size criterion is discussed in Appendix B. The criterion used states that the natural frequency of a simple supported beam element must be greater than 50 Hz. If this criterion was not met an intermediate grid point was added. For the diagonals, with the length between ball joints used, the natural frequency was 20.5 Hz and with one intermediate grid point at the center the frequency was 82 Hz. The additional quarter point locations were added because of the actual ball-joint boundary conditions at the diagonal ends; the criterion is actually intended for structures with built in ends.

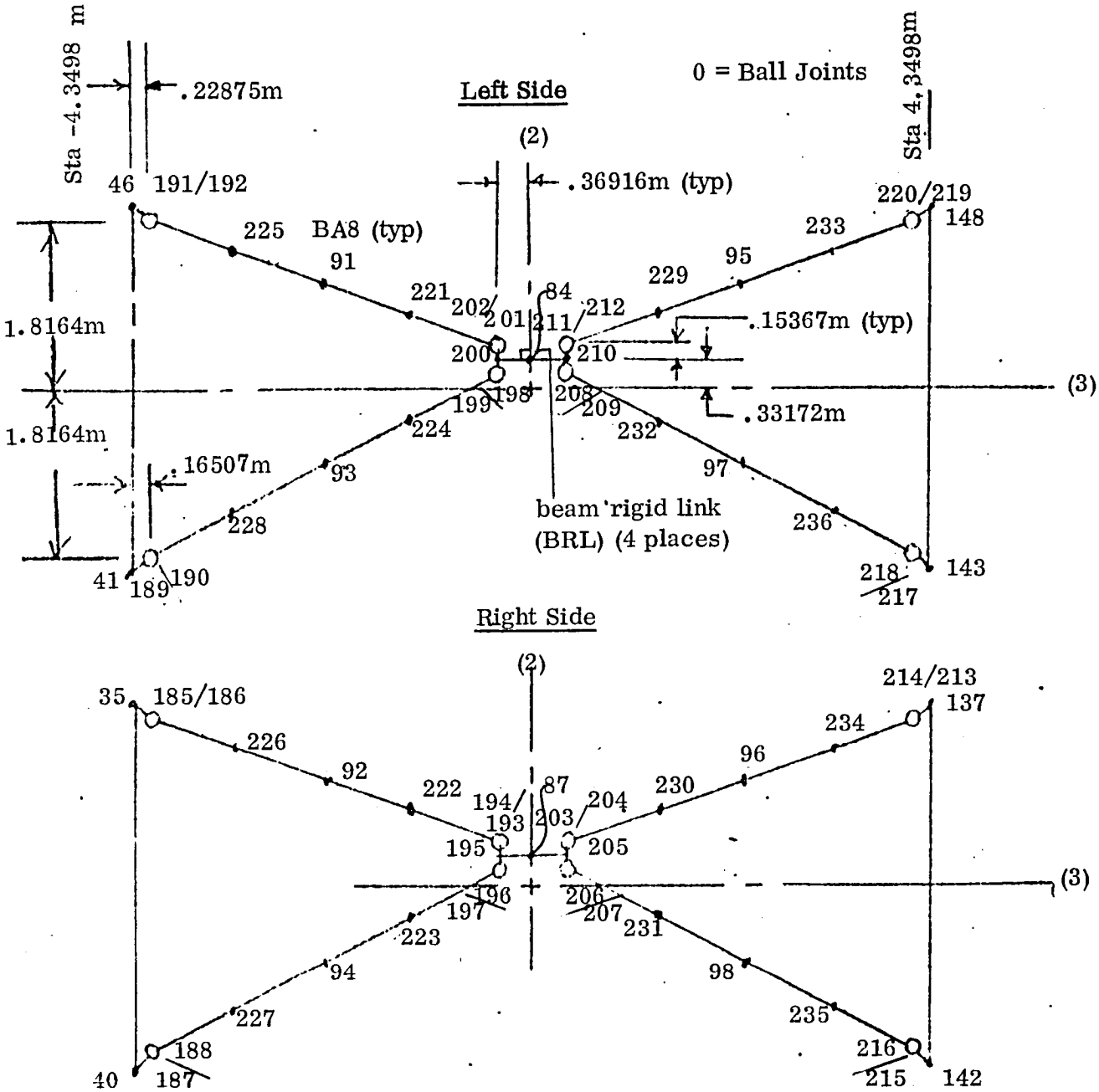

All intermediate grid points are at 1/4 points

Lateral Locations (1) GP 193-212 at ± 1.8796m
GP 185, 186, 191, 192, 213, 214, 219 & 220 at ± .63391m
GP 187-190, 215-218 at ± .61468m

SPAR Section Properties (Table 9)	No. of Elements
BA8	32 - 15.24 cm (6 in) tube (all main diagonal elements)
BA19	4 - flat plate 2.54 x 18.288 cm (1.0 x 7.2 in) with 18.542 cm (7.3 in) BRL at grid point 84 and 87.
BA20	16 - flat plate 1.905 x 17.78 cm (.75 x 7.0 in) connecting ball joints to grid points 195, 200, 205, 210, 35, 40, 41, 46, 137, 142, 143 & 148

Figure 17. Diagonals

Cross Beam

The cross beam shown in Figure 18 was the seventh substructure group modeled. This group consists of 13 beam elements and one zero length beam element, E25 , between grid points 9 and 184 to represent the pin joint. The spar input stiffness matrix, BB, was of the form of equation (5) for a pin joint about the 3 axis. All values on the diagonal of the stiffness matrix were given a value of 700508 MN/m or a value at least two orders of magnitude larger than the bending stiffness of the spindle pin (3 elements connecting grid points 184 to 28). The error in the bending deflection of a simple cantelever beam in series with a rigid link using equation (4) was less than one tenth of one percent. The four lateral tubes have relatively stiff end fittings. The fittings were made rigid by using beam rigid link offsets so that the flexible tube lengths were correct. The upright beam elements connecting grid points 3 to 9 and 7 to 9 are of a complex I beam configuration seen in Figure 3. The torsional stiffness due to differential bending was added to the basic torsional stiffness of these beam elements. The basic section had a torsional stiffness of 105.7 cm^4 compared with the differential-bending torsional stiffness of 1111. cm^4. This stiffness controls the frequency of the first flexible mode.

The SPAR input stiffness matrix, BB , was of the form

$$K = \begin{bmatrix} K_{11} & 0 & 0 & 0 & 0 & 0 \\ 0 & K_{22} & 0 & 0 & 0 & 0 \\ 0 & 0 & K_{33} & 0 & 0 & 0 \\ 0 & 0 & 0 & K_{44} & 0 & 0 \\ 0 & 0 & 0 & 0 & K_{55} & 0 \\ 0 & 0 & 0 & 0 & 0 & 0 \end{bmatrix} \quad (5)$$

for a pin joint about the 3 axis.

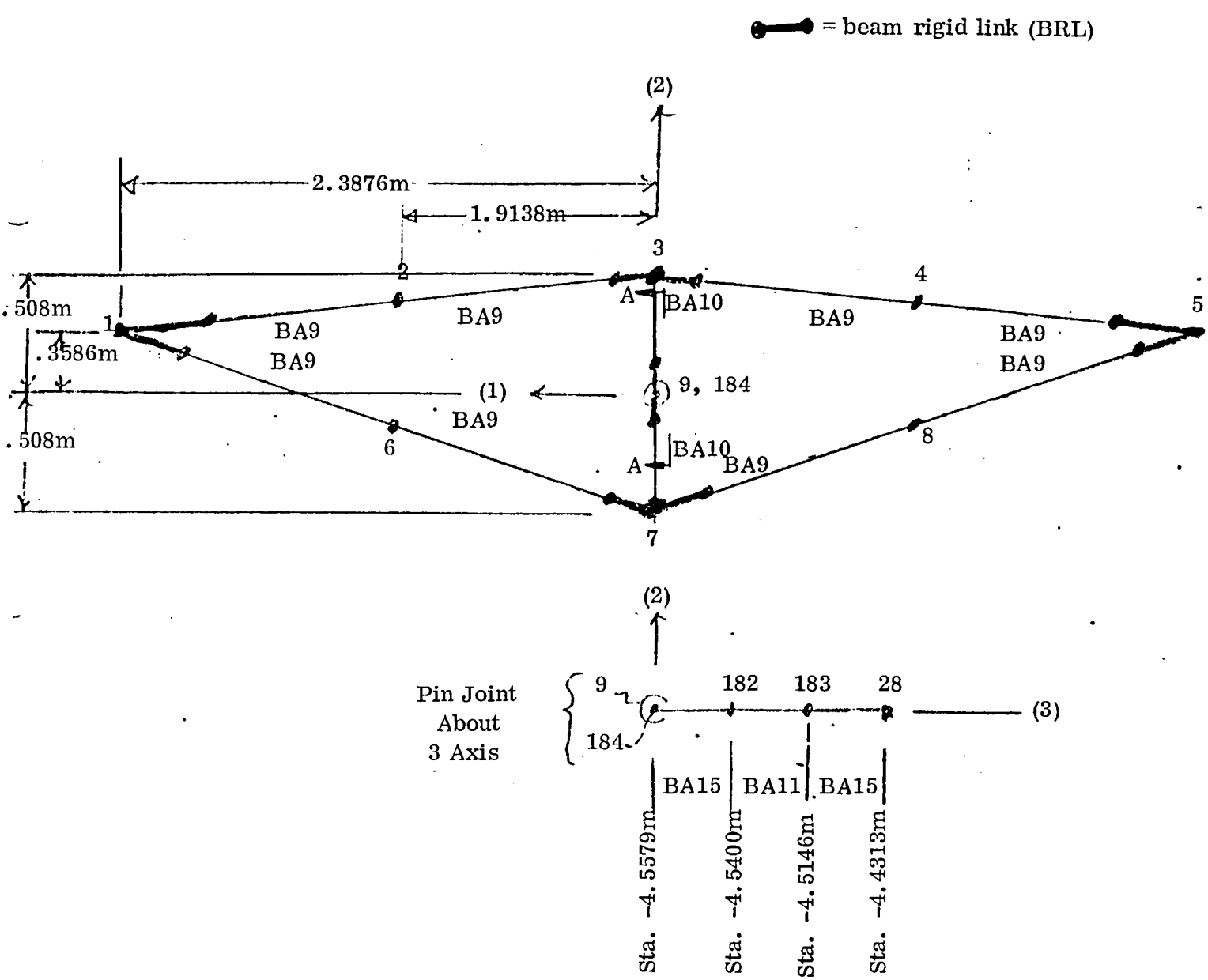

Section A-A

SPAR Section Properties (Table 9)	No. of Elements
BA9	8 - lateral members are 10.16 cm (4 in) dia. tubes
BA10	2 - built up section, torsion stiffness includes differential bending
BA11	1 - complex flexible section at center of spindle pin
BA15	2 - solid circular shaft

Figure 18. Cross Beam at Station - 4.4313 m

IECM Shelf

The eighth substructure group was the IECM shelf structure consisting of 21 beam elements and 6 quadrilateral plate elements as shown in Figure 19. Grid points 85, 86, 99 and 100 are located on the center bulkhead. The 5.08 cm (2. in) diameter diagonal tubes support the IECM shelf off of the center bulkhead. The outer frame and the support beams at stations .2794 m and .9906 m are made of channel sections. The other panel stiffeners at stations .5364 m, .7396 m and 1.2002 m are angle beam elements. There are six .160 cm (.063 in) thick quadrilateral plate elements.

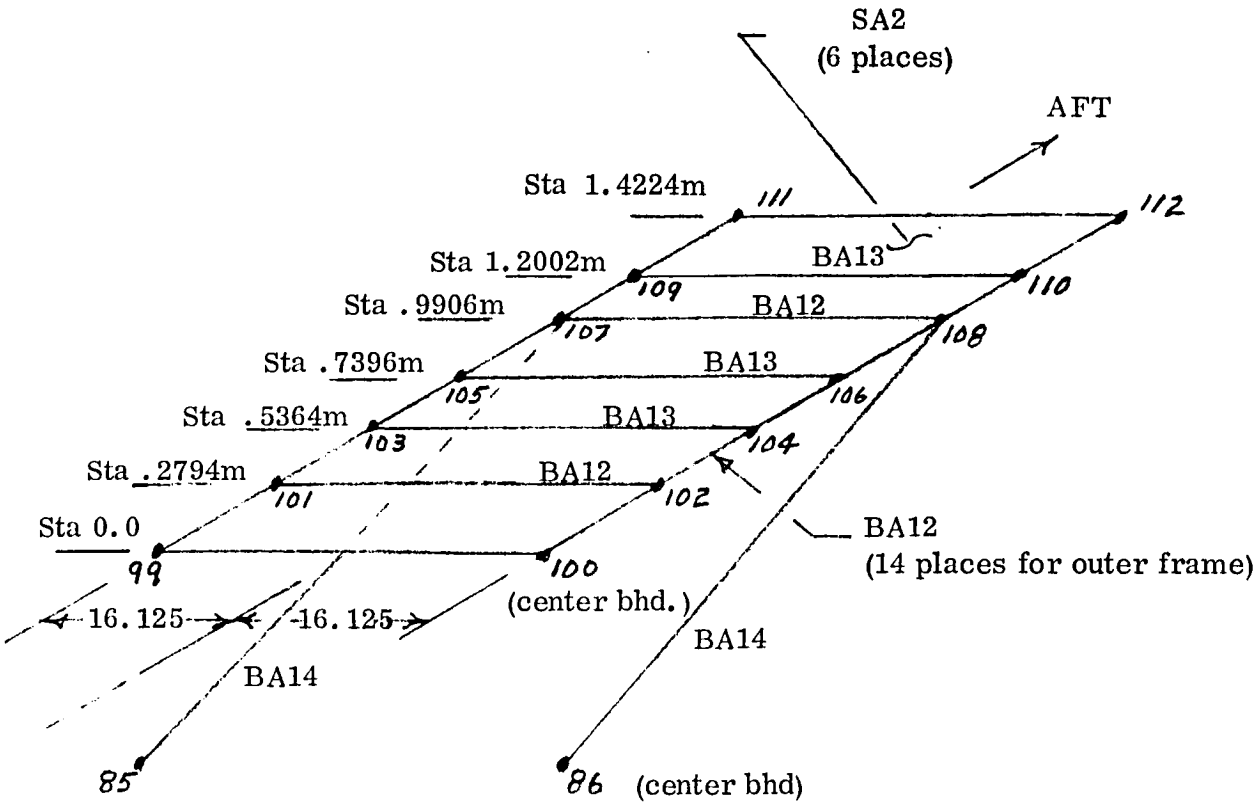

SPAR Section Properties (Table 9)	No. of Elements
BA12	16 - 7.62 x 4.445 cm (3. x 1.75 in) channel
BA13	3 - 2.54 x 2.2352 cm (1. x .88 in) angle
BA14	2 - 5.08 cm (2. in) dia. tube
SA2	6 - .160 cm (.063 in) plate

Figure 19. IECM Shelf

Experiment Trays

The ninth and final substructure group included the 86 experiment trays that were modeled as equivalent orthotropic panel elements as depicted in Figure 20. A static SPAR tray model was used to obtain the six by six panel stiffness matrix for each type of tray. Figure 21 shows the tray locations.

Types of Tray	Tray Depth	Figure 21 Code
Side Trays		
Debris experiment	7.62 cm (3 in)	DP
Shallow	7.62 cm (3 in)	S
Nominal	15.24 cm (6 in)	N
Deep	30.48 cm (12 in)	D
End Trays		
Shallow rectangular	7.62 cm (3 in)	SR
Nominal rectangular	15.24 cm (6 in)	NR
Deep rectangular	30.48 cm (12 in)	DR
Shallow square (corner)	7.62 cm (3 in)	SC
Nominal square (corner)	15.24 cm (6 in)	NC
Deep square (corner)	30.48 cm (12 in)	DC

As shown in Figure 20 there is coupling between extensional and bending terms as well as between the shear and twisting terms. Figure 22 shows the extentional-bending coupling of a shallow side tray. Figure 23 shows the shear-twisting coupling of the base plate of a deep side tray. In Figure 21 each rectangle represents a tray with the type of tray in the upper left hand corner and the total tray weight in the lower right hand corner. The bay location and the row numbers are also shown in Figure 21. The tray model shown in Figure 20 is the Debris experiment tray. All of the four side tray types were modeled and the nominal and deep rectangular end trays were modeled.

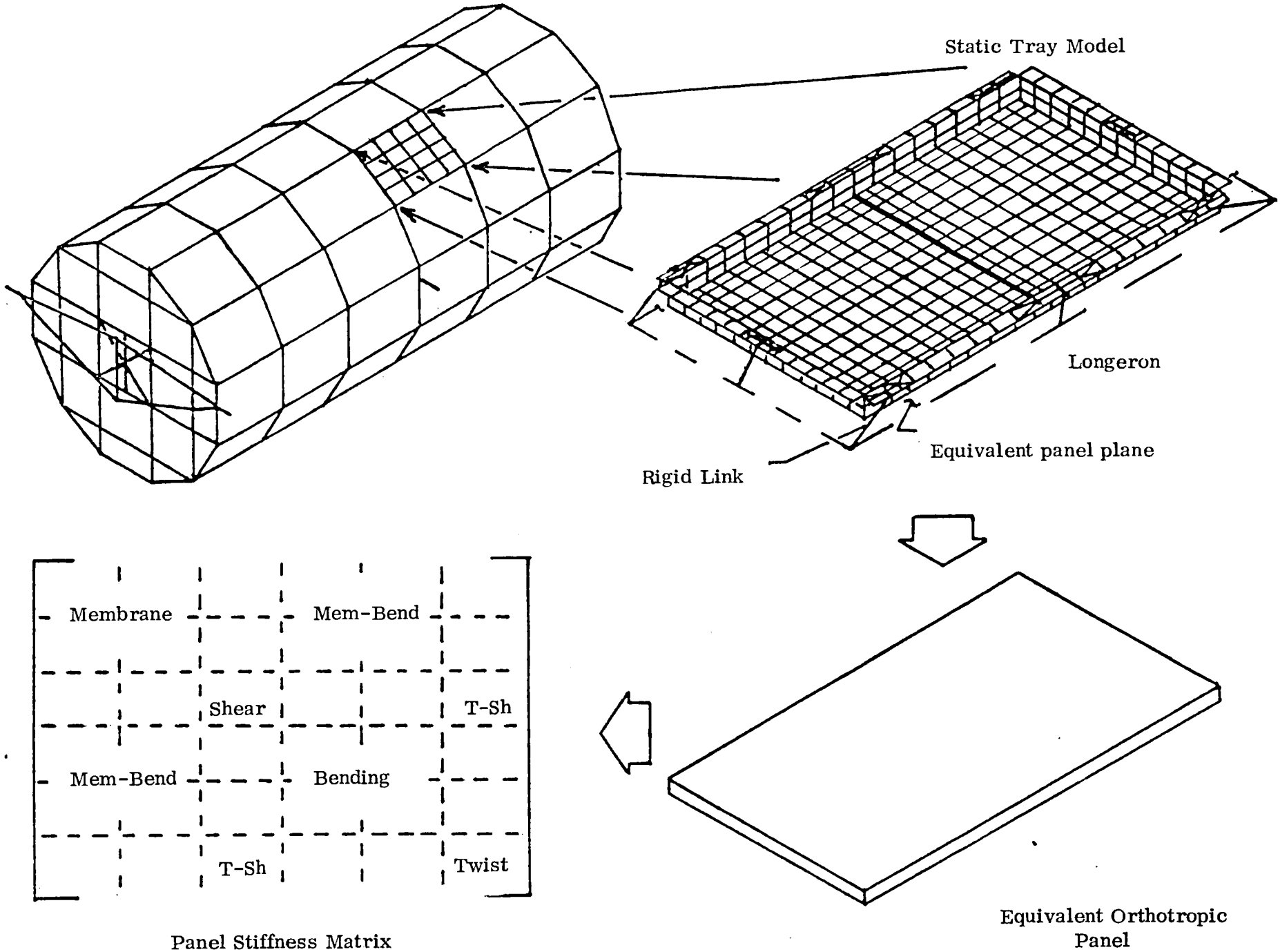

Figure 20. SPAR Model of LDEF Experiment Tray

Bay Row	A	B	C	D	E	F
1	DP 24.95	DP 24.95	S 36.29	S 102.06	S 44.45	S 44.45
2	N 101.60	D 100.70	DP 24.95	DP 24.95	D 100.70	S 39.92
3	S 79.83	N 101.60	S 54.88	DP 24.95	S 93.44	N 68.49
4	N 101.60	S 36.29	DP 51.71	S 102.06	N 101.60	DP 24.95
5	DP 24.95	D 100.70	S 70.31	DP 24.95	D 100.70	S 39.92
6	DP 24.95	S 41.28	N 101.60	N 101.60	S 56.25	N 41.73
7	S 44.45	D 100.70	DP 24.95	DP 24.95	D 100.70	DP 24.95
8	DP 24.95	S 36.29	S 102.06	S 102.06	N 101.60	S 72.12
9	N 101.60	S 98.43	S 49.89	DP 24.95	N 101.60	N 58.49
10	N 101.60	D 64.41	S 36.29	DP 51.71	D 100.70	DP 24.95
11	DP 24.95	DP 24.95	S 102.06	S 102.06	DP 24.95	DP 24.95
12	DP 63.05	S 36.29	S 61.69	D 163.75	D 43.09	N 76.20

Center Bhd.

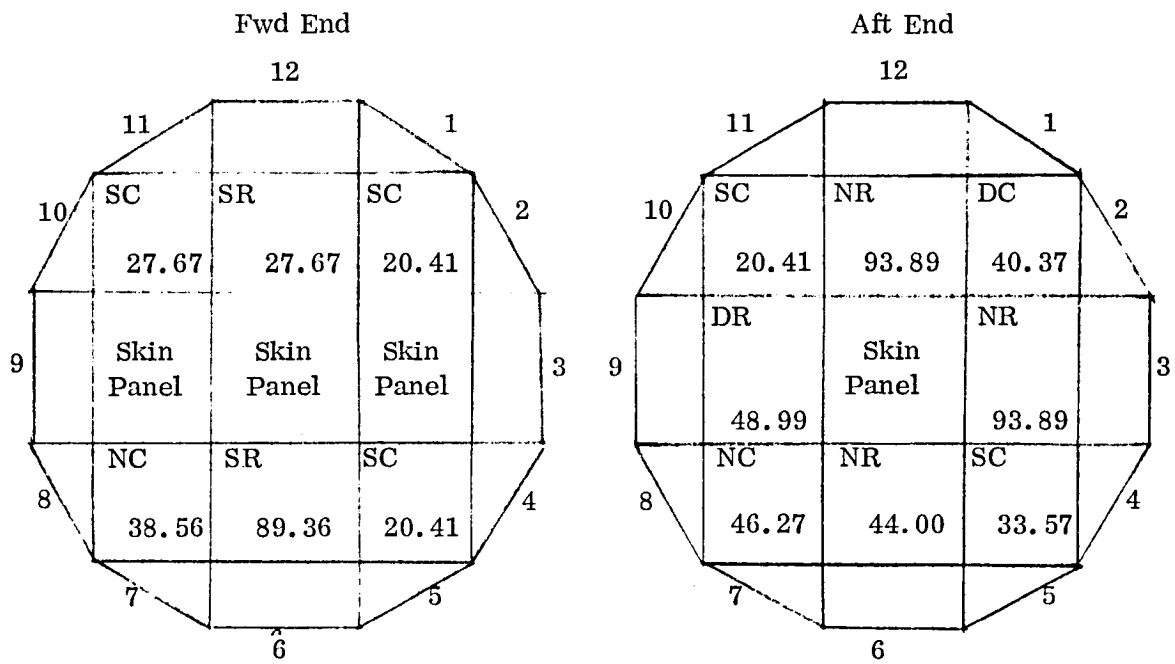

Figure 21. Tray Locations and Total Weight (kg) (See Figure 1)

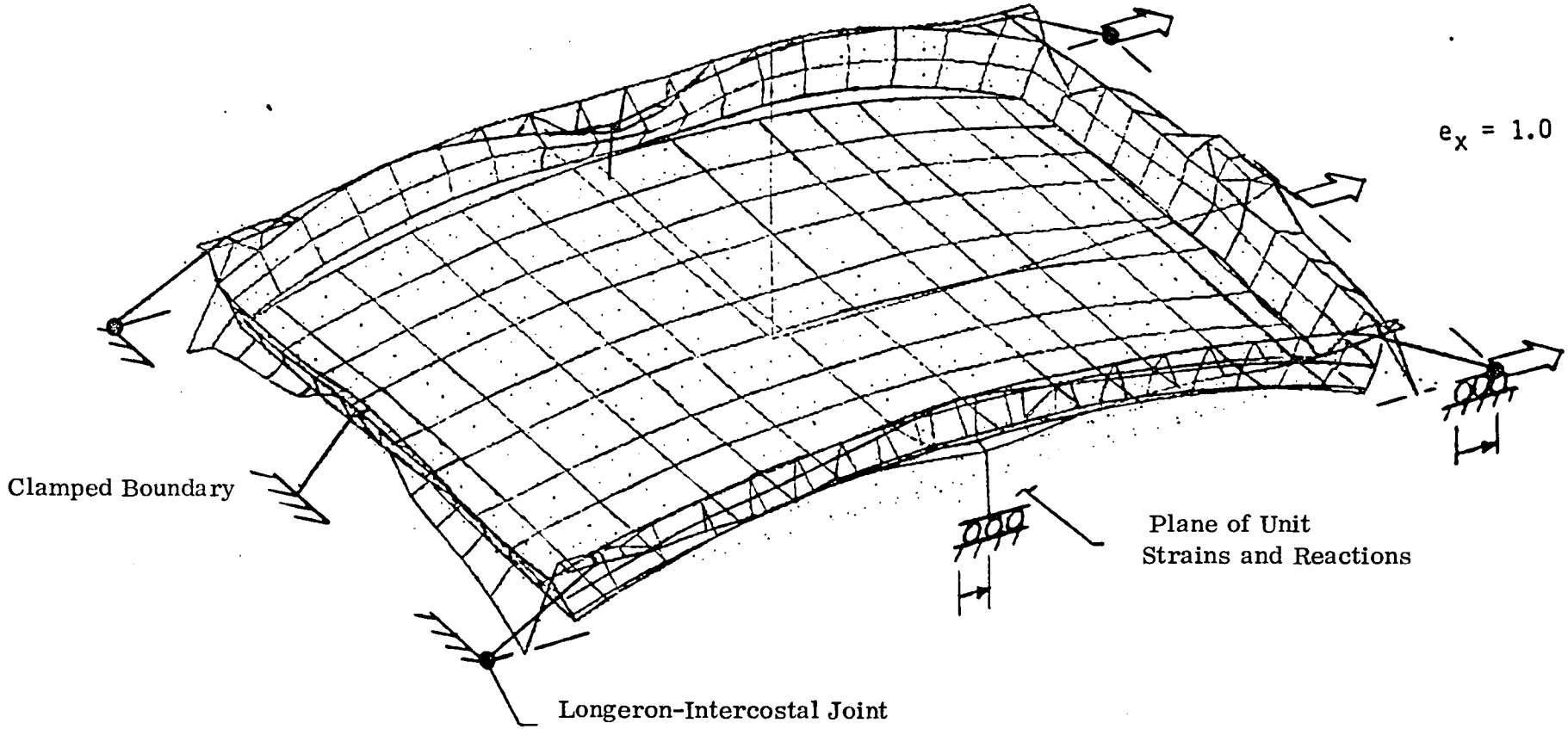

Figure 22. Static Deformation of Tray Under Unit Longitudinal Strain

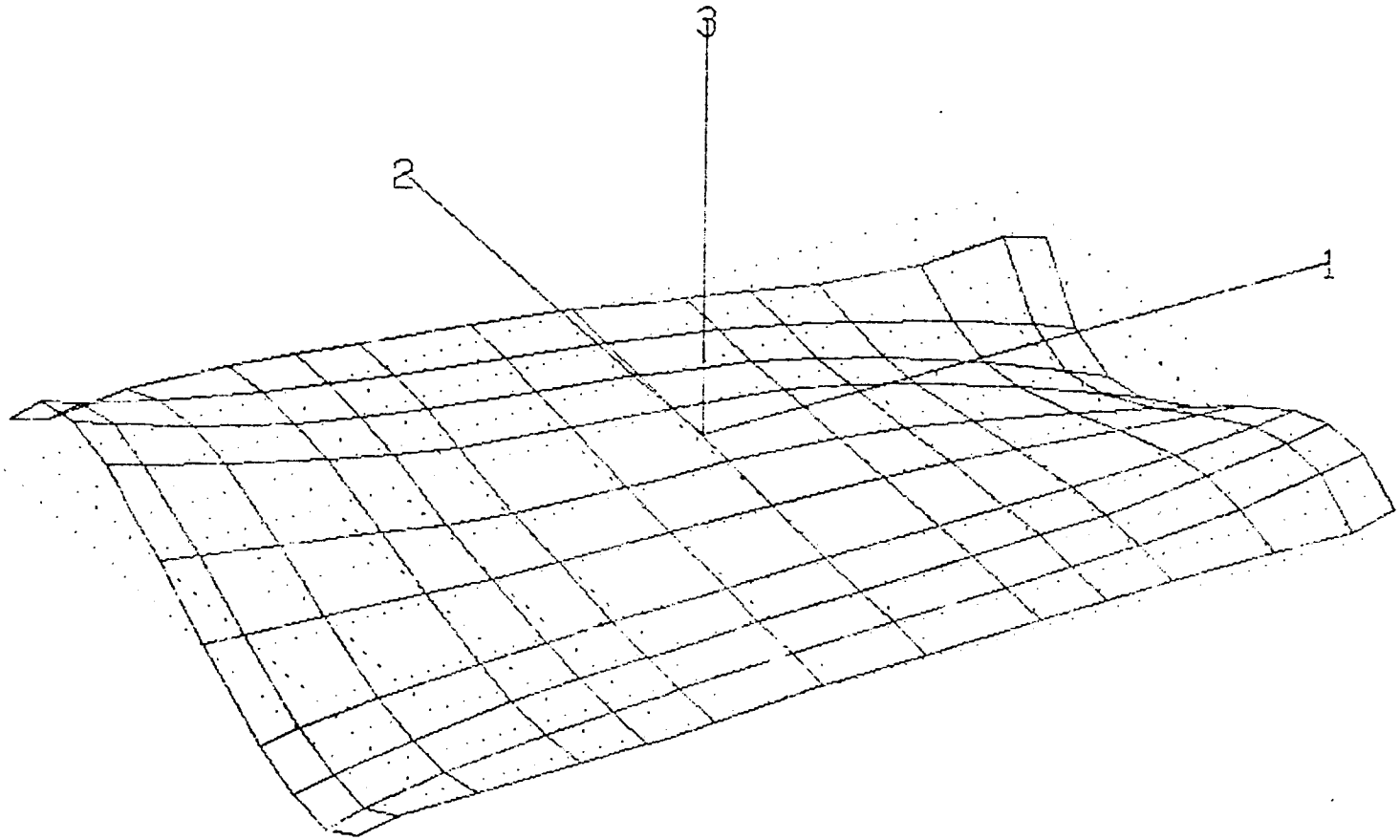

Figure 23. Shear-Twisting Coupling of the Deep Side Tray Base Plate
(Shear Strain Equal to Unity)

TRAY EFFECTIVE PANEL STIFFNESS PROPERTIES

Stiffness Matrix From SPAR Tray Models

The flanges of the side trays are clamped to the structure at 8 locations as shown in Figure 8. Rigid links were used to connect these 8 clamping points on the tray lip to the plane of the four corner longeron grid points and to four points mid way between these grid points.

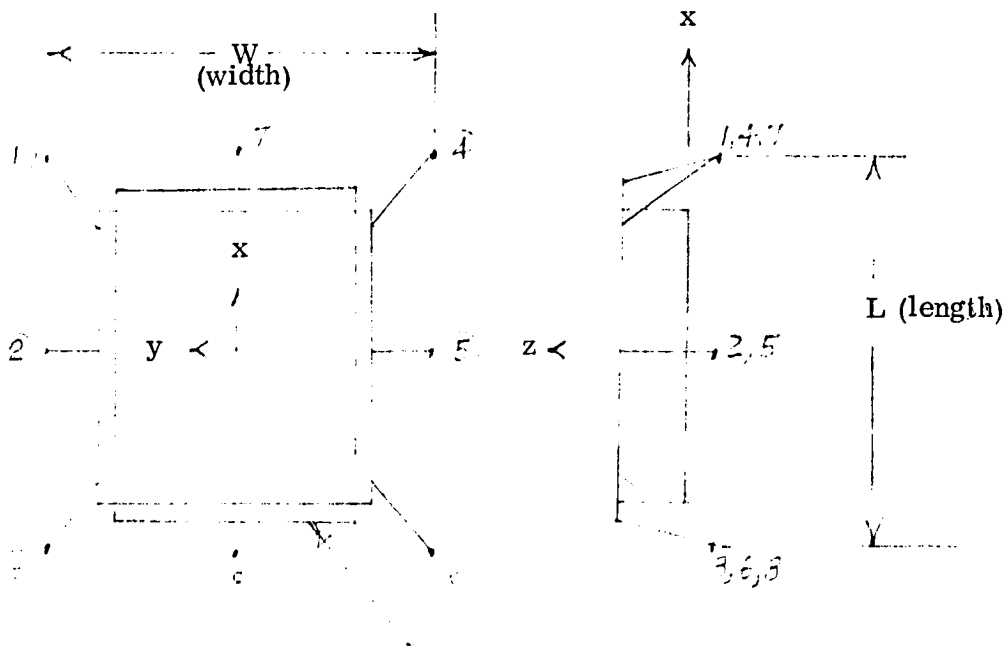

Tray grid points 1, 3, 4 and 6 are at the actual location of the LDEF longeron grid points. Tray grid points 2, 5, 7 and 8 are located midway between the longeron grid points.

The SPAR panel stiffness matrix is of the form

$$\begin{Bmatrix} N_x \\ N_y \\ N_{xy} \\ M_x \\ M_y \\ M_{xy} \end{Bmatrix} = \begin{bmatrix} C_{11} & C_{12} & 0 & C_{14} & C_{15} & 0 \\ C_{21} & C_{22} & 0 & C_{24} & C_{25} & 0 \\ 0 & 0 & C_{33} & 0 & 0 & C_{36} \\ C_{41} & C_{42} & 0 & C_{44} & C_{45} & 0 \\ C_{51} & C_{52} & 0 & C_{54} & C_{55} & 0 \\ 0 & 0 & C_{63} & 0 & 0 & C_{66} \end{bmatrix} \begin{Bmatrix} e_x \\ e_y \\ e_{xy} \\ k_x \\ k_y \\ k_{xy} \end{Bmatrix} \quad (6)$$

where

$$k_x = -\frac{\partial^2 w}{\partial x^2} \quad , \quad k_y = -\frac{\partial^2 w}{\partial y^2} \quad , \quad k_{xy} = 2\frac{\partial^2 w}{\partial x \, \partial y}$$

Each column of this stiffness matrix was obtained by setting one of the strains equal to unity and all others equal to zero. The six resulting conditions are the longitudinal strain equals unity ($e_x = 1.0$), the lateral strain equals unity ($e_y = 1.0$) , the shear strain equals unity ($e_{xy} = 1.0$), the longitudinal rotation equals unity ($k_x = 1.0$), the lateral rotation equals unity ($k_y = 1.0$), and the twisting rotation equals unity ($k_{xy} = 1.0$). Table 2 shows the actual displacements imposed on the tray model at the ends of the rigid links for each of the six displacement conditions. The force reactions output at grid points 1 through 8 were used to determine the stiffness coefficients in equation (6). The stress resultants on the left side of equation (6) can be expressed as functions of these reaction forces.

Using the SPAR panel sign convention

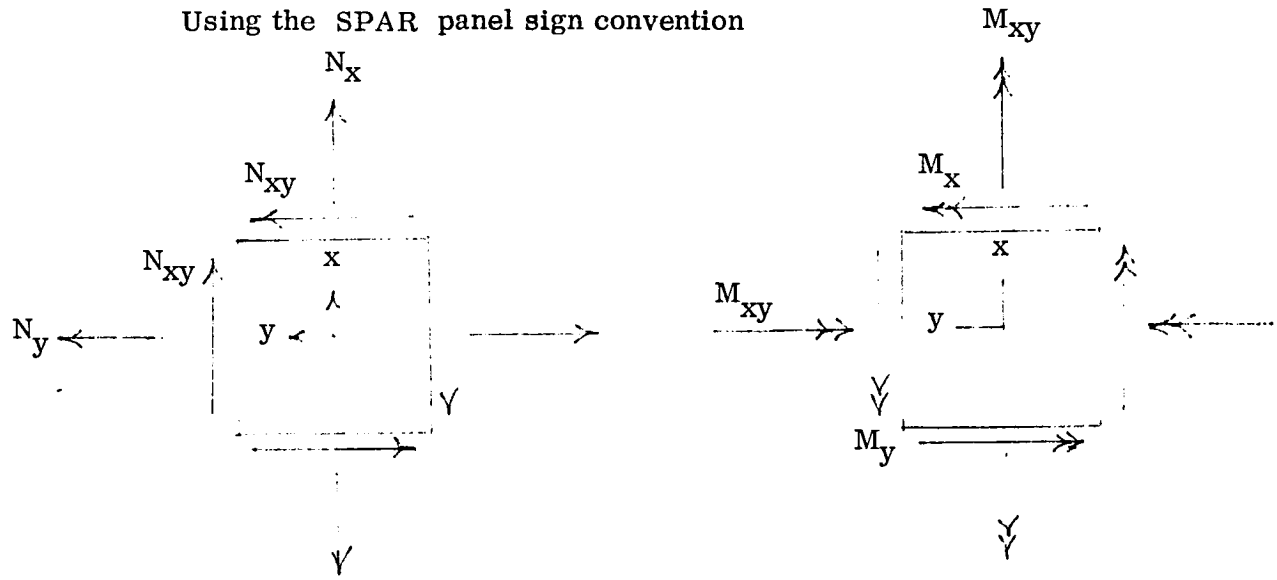

$$N_x = \frac{P_{1x} + P_{7x} + P_{4x}}{W}$$

$$N_y = \frac{P_{1y} + P_{2y} + P_{3y}}{L}$$

$$N_{xy} = \frac{P_{1y} + P_{7y} + P_{4y}}{W} + \frac{\sum_{i=1}^{8} (M_z)_i}{2 L W}$$

SPAR Reaction Sign Convention

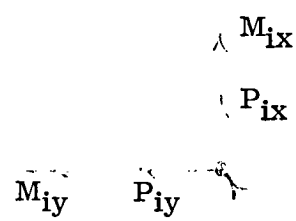

where

$$
\begin{aligned}
& \text{or} \\
N_{xy} &= \frac{P_{1x} + P_{2x} + P_{3x}}{L} - \frac{\Sigma M_z}{2\,L\,W} \\
M_x &= \frac{M_{1y} + M_{7y} + M_{4y}}{W} \\
M_y &= \frac{-M_{1x} - M_{2x} - M_{3x}}{L} \\
M_{xy} &= \frac{-M_{1y} - M_{2y} - M_{3y}}{L} + \frac{P_{1z} - P_{3z}}{4} \\
& \text{or} \\
M_{xy} &= \frac{M_{1x} + M_{7x} + M_{4x}}{W} + \frac{P_{1z} - P_{4z}}{4}
\end{aligned}
\tag{7}
$$

where

P_{ij} Reaction Force

M_{ij} Reaction Moment

Subscript i is the grid point number

Subscript j is the tray coordinate direction

L Length of effective panel

W Width of effective panel

From equation (6) and the boundary conditions in Table 2 the values of the stiffness matrix are calculated by inserting the reaction forces and moments into equation (7). The first column of the stiffness matrix is obtained by setting $e_x = 1.0$ in equation (6) and all others equal to zero.

$$
\begin{aligned}
& e_x = 1.0 \qquad\qquad\qquad\qquad e_y = 1.0 \\
\{N\} &= \begin{Bmatrix} N_x \\ N_y \\ N_{xy} \\ M_x \\ M_y \\ M_{xy} \end{Bmatrix} = \begin{Bmatrix} C_{11} \\ C_{21} \\ 0 \\ C_{41} \\ C_{51} \\ 0 \end{Bmatrix} \qquad \{N\} = \begin{Bmatrix} C_{12} \\ C_{22} \\ 0 \\ C_{42} \\ C_{52} \\ 0 \end{Bmatrix}
\end{aligned}
\tag{8}
$$

for $e_{xy} = 1.0$

$$\{N\} = \begin{Bmatrix} 0 \\ 0 \\ C_{33} \\ 0 \\ 0 \\ C_{63} \end{Bmatrix}$$

for $k_x = 1.0$

$$\{N\} = \begin{Bmatrix} C_{14} \\ C_{24} \\ 0 \\ C_{44} \\ C \\ 0 \end{Bmatrix}$$

for $k_y = 1.0$

$$\{N\} = \begin{Bmatrix} C_{15} \\ C_{25} \\ 0 \\ C_{45} \\ C_{55} \\ 0 \end{Bmatrix}$$

for $k_{xy} = 1.0$

$$\{N\} = \begin{Bmatrix} 0 \\ 0 \\ C_{36} \\ 0 \\ 0 \\ C_{66} \end{Bmatrix}$$

The design of the tray-to-structure clamp allowed in plane relative sliding motion between the tray flange and the mounting structure. The four side mid point clamps were allowed some relative motion by letting θ_z be free to rotate at grid point 2, 5, 7 and 8. This is shown in Table 2 for the shear ($e_{xy} = 1.0$) and the twisting ($k_{xy} = 1.0$) boundary conditions. By allowing this flange motion the shear and twisting stiffnessos are reduced to 54 and 58 percent of the values for the original boundary conditions, as shown in Appendix A.

To demonstrate the procedure, the numerical results from the evaluation of the Debris tray subjected to a longitudinal strain equal to unity ($e_x = 1.0$) will be shown in the following discussion. The reaction forces and moments from the SPAR static run are shown below.

REACTION FORCES (MN)

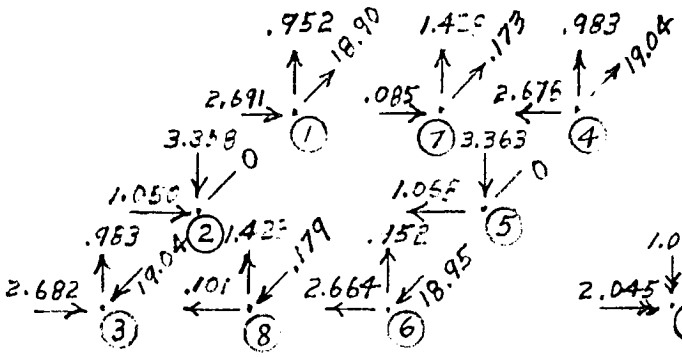

REACTION MOMENTS (Mm-N)

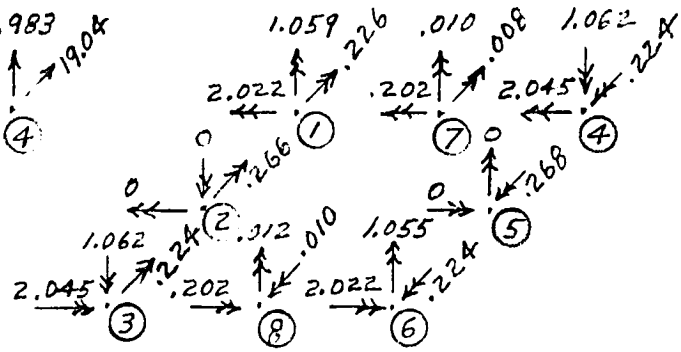

With a panel length (L) of 1.5304 m (60.25 in) and a panel width (W) of 1.0584 m (41.6698 in) the stress resultants from equations (7) and (8) result in the first column of the stiffness matrix

$$
\begin{aligned}
N_x &= C_{11} = .3604 \text{ MN/cm} \\
N_y &= C_{21} = -.04186 \text{ MN/cm} \\
N_{xy} &= C_{31} = 0.0 \\
M_x &= C_{41} = 4.034 \text{ MN} \\
M_y &= C_{51} = -.4675 \text{ MN} \\
M_{xy} &= C_{61} = 0.0
\end{aligned}
$$

All of the other five static boundary displacements are imposed on the same tray model to obtain the six-by-six stiffness matrix.

Original Debris Tray Stiffness Matrix (MN/cm, MN & Mm - N)

$$
\begin{Bmatrix} N_x \\ N_y \\ N_{xy} \\ M_x \\ M_y \\ M_{xy} \end{Bmatrix} = \begin{bmatrix} .3604 & -.04186 & 0 & 2.522 & -.1953 & 0 \\ -.04186 & .08170 & 0 & -.1085 & .7397 & 0 \\ 0 & 0 & .05594 & 0 & 0 & -.2264 \\ 4.034 & -.4319 & 0 & .2564 & -.02164 & 0 \\ -.4675 & .8332 & 0 & -.01165 & .07187 & 0 \\ 0 & 0 & -.2264 & 0 & 0 & .009610 \end{bmatrix} \begin{Bmatrix} e_x \\ e_y \\ e_{xy} \\ k_x \\ k_y \\ k_{xy} \end{Bmatrix}
$$

Because some of the off diagonal terms are not equal, the average values were taken resulting in the final stiffness matrix for the Debris tray of

$$
\begin{Bmatrix} N_x \\ N_y \\ N_{xy} \\ M_x \\ M_y \\ M_{xy} \end{Bmatrix} = \begin{bmatrix} .3604 & -.04186 & 0 & 3.278 & -.3314 & 0 \\ -.04186 & .08170 & 0 & -.2702 & .7864 & 0 \\ 0 & 0 & .05594 & 0 & 0 & -.2264 \\ 3.278 & -.2702 & 0 & .2564 & -.01664 & 0 \\ -.3314 & .7864 & 0 & -.01664 & .07187 & 0 \\ 0 & 0 & -.2264 & 0 & 0 & .009610 \end{bmatrix} \begin{Bmatrix} e_x \\ e_y \\ e_{xy} \\ k_x \\ k_y \\ k_{xy} \end{Bmatrix}
$$

The final stiffness values used in all the equivalent panels are tabulated in Appendix A.

The units for the stiffness matrix are partitioned as

$$\begin{Bmatrix} N_x \\ N_y \\ N_{xy} \\ \hline M_x \\ M_y \\ M_{xy} \end{Bmatrix} = \left[\begin{array}{ccc|ccc} & \text{MN/cm} & & & \text{MN} & \\ & & & & & \\ & & & & & \\ \hline & \text{MN} & & & \text{Mm-N} & \end{array}\right] \begin{Bmatrix} e_x \\ e_y \\ e_{xy} \\ \hline k_x \\ k_y \\ k_{xy} \end{Bmatrix}$$

TABLE 2. DISPLACEMENT BOUNDARY CONDITIONS FOR TRAY STATIC MODELS

e_x = UNITY

	u_x	u_y	u_z	θ_x	θ_y	θ_z
1	L	0	0	0	0	0
2	F	0	0	0	0	0
3	0	0	0	0	0	0
4	L	0	0	0	0	0
5	F	0	0	0	0	0
6	0	0	0	0	0	0
7	L	0	0	0	0	0
8	0	0	0	0	0	0

e_y = UNITY

	u_x	u_y	u_z	θ_x	θ_y	θ_z
1	0	W	0	0	0	0
2	0	W	0	0	0	0
3	0	W	0	0	0	0
4	0	0	0	0	0	0
5	0	0	0	0	0	0
6	0	0	0	0	0	0
7	0	F	0	0	0	0
8	0	F	0	0	0	0

e_{xy} = UNITY

	u_x	u_y	u_z	θ_x	θ_y	θ_z
1	W/4	L/4	0	0	0	0
2	W/4	0	0	0	0	F
3	W/4	-L/4	0	0	0	0
4	-W/4	L/4	0	0	0	0
5	-W/4	0	0	0	0	F
6	-W/4	-L/4	0	0	0	0
7	0	L/4	0	0	0	F
8	0	-L/4	0	0	0	F

k_x = UNITY

	u_x	u_y	u_z	θ_x	θ_y	θ_z
1	0	0	0	0	L/2	0
2	0	0	h	0	0	0
3	0	0	0	0	-L/2	0
4	0	0	0	0	L/2	0
5	0	0	h	0	0	0
6	0	0	0	0	-L/2	0
7	0	0	0	0	L/2	0
8	0	0	0	0	-L/2	0

k_y = UNITY

	u_x	u_y	u_z	θ_x	θ_y	θ_z
1	0	0	0	W/2	0	0
2	0	0	0	W/2	0	0
3	0	0	0	W/2	0	0
4	0	0	0	-W/2	0	0
5	0	0	0	-W/2	0	0
6	0	0	0	-W/2	0	0
7	0	0	h	0	0	0
8	0	0	h	0	0	0

k_{xy} = UNITY

	u_x	u_y	u_z	θ_x	θ_y	θ_z
1	0	0	WL/16	L/8	-W/8	0
2	0	0	0	0	-W/8	F
3	0	0	-WL/16	-L/8	-W/8	0
4	0	0	-WL/16	L/8	W/8	0
5	0	0	0	0	W/8	F
6	0	0	WL/16	-L/8	W/8	0
7	0	0	0	L/8	0	F
8	0	0	0	-L/8	0	F

W = width L = length

F = free boundary h = calculated height of a circular arch at the mid point

Extrapolation of Rectangular End Tray Stiffness

Because the end bulkhead structure is of a rigid welded I beam configuration, the end tray panel stiffness will have a minor effect on the LDEF dynamic response. For this reason only two of the end trays were modeled, the nominal and deep rectangular trays, and the stiffness for the other trays were extrapolated from this data. The value of each stiffness term of the shallow tray rectangular matrix (C_3) was extrapolated linearly from the nominal (C_6) and deep (C_{12}) rectangular stiffness terms:

$$C_3 = C_6 - (C_{12} - C_6) = 2 C_6 - C_{12} \tag{9}$$

Tray Panel Effective Properties

The construction and clamping of the rectangular and square end trays were very similar so the following set of equations were used to obtain the square trays stiffness matrix knowing that the x and y direction properties must be equal. The effective tray panels can be represented as orthotropic panels that have membrane-bending coupling and twisting - shear coupling because of rigid link offsets.

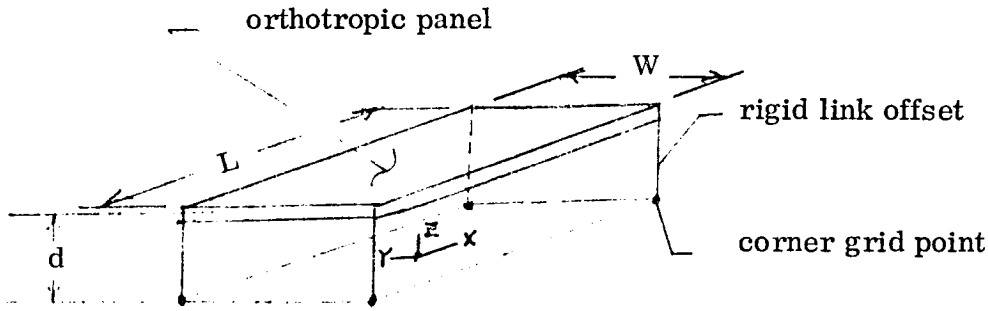

The orthotropic stiffness matrix has the form:

$$\begin{Bmatrix} N_x \\ N_y \\ N_{xy} \\ M_x \\ M_y \\ M_{xy} \end{Bmatrix} = \begin{bmatrix} C_{11} & C_{12} & 0 & 0 & 0 & 0 \\ C_{21} & C_{22} & 0 & 0 & 0 & 0 \\ 0 & 0 & C_{33} & 0 & 0 & 0 \\ 0 & 0 & 0 & C_{44} & C_{45} & 0 \\ 0 & 0 & 0 & C_{54} & C_{55} & 0 \\ 0 & 0 & 0 & 0 & 0 & C_{66} \end{bmatrix} \begin{Bmatrix} e_x \\ e_y \\ e_{xy} \\ k_x \\ k_y \\ k_{xy} \end{Bmatrix} \qquad (10)$$

Because of the offset (d_x) there are coupled loadings in the xz plane.

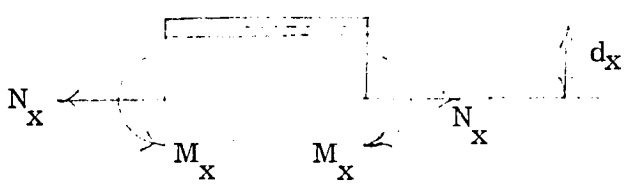

$$M_x = d_x N_x \qquad (11)$$

For coupled loadings in the yz plane,

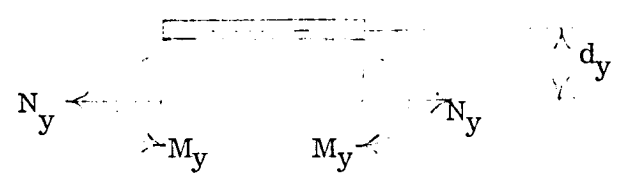

$$M_y = d_y N_y$$

For coupled loadings in the x = L/2 plane,

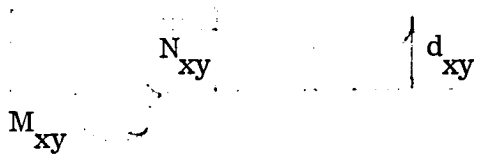

$$M_{xy} = -d_{xy} N_{xy}$$

Using these coupling equations, the left side of equation (6) can be rewritten.

$$\begin{Bmatrix} N_x \\ N_y \\ N_{xy} \\ d_x N_x \\ d_y N_y \\ -d_{xy} N_{xy} \end{Bmatrix} = \begin{bmatrix} C_{11} & C_{12} & 0 & C_{14} & C_{15} & 0 \\ C_{21} & C_{22} & 0 & C_{24} & C_{25} & 0 \\ 0 & 0 & C_{33} & 0 & 0 & C_{36} \\ C_{41} & C_{42} & 0 & C_{44} & C_{45} & 0 \\ C_{51} & C_{52} & 0 & C_{54} & C_{55} & 0 \\ 0 & 0 & C_{63} & 0 & 0 & C_{66} \end{bmatrix} \begin{Bmatrix} e_x \\ e_y \\ e_{xy} \\ k_x \\ k_y \\ k_{xy} \end{Bmatrix} \tag{12}$$

By equating the first row equation with the fourth row

$$d_x = \frac{C_{41}e_x + C_{42}e_y + C_{44}k_x + C_{45}k_y}{C_{11}e_x + C_{12}e_y + C_{14}k_x + C_{15}k_y} \tag{13}$$

By equating the second row and fifth row equation

$$d_y = \frac{C_{51}e_x + C_{52}e_y + C_{54}k_x + C_{55}k_y}{C_{21}e_x + C_{22}e_y + C_{24}k_x + C_{25}k_y}$$

By equating the third row and sixth row equation

$$d_{xy} = -\frac{C_{63}e_{xy} + C_{66}k_{xy}}{C_{33}e_{xy} + C_{36}k_{xy}}$$

The three load coupling offsets d_x, d_y and d_{xy} change with changes in the boundary strain conditions. For extrapolating purposes these equations were

reduced to the following by using the boundary conditions:

$$\frac{e_x = 1,\ e_y = k_x = k_y = 0}{d_x = \frac{C_{41}}{C_{11}}}$$

$$\frac{e_y = 1,\ e_x = k_x = k_y = 0}{d_y = \frac{C_{52}}{C_{22}}} \qquad (14)$$

$$\frac{e_{xy} = 1,\ k_{xy} = 0}{d_{xy} = -\frac{C_{63}}{C_{33}}}$$

Using the orthotropic equations for composites from Reference 3, the values of the Poisson's Ratios and the extensional and shear effective thicknesses for each type of panel can be derived.

$$\nu_{yx} = \frac{C_{12}}{C_{11}}$$

$$\nu_{xy} = \frac{C_{12}}{C_{22}}$$

$$t_x = \frac{C_{11}}{E}(1 - \nu_{xy}\nu_{yx}) \qquad (15)$$

$$t_y = \frac{C_{22}}{E}(1 - \nu_{xy}\nu_{yx})$$

$$t_{xy} = \frac{C_{33}}{G}$$

From equations(14) and (15) the orthotropic properties and the offsets of each tray type are tabulated in Table 3.

Extrapolation of Square End Tray Stiffness

For the square end trays the following set of stiffness terms were used*:

$$d_x' = d_y' = \frac{d_x + d_y}{2}$$

$$C_{11}' = C_{22}' = \frac{C_{11} + C_{22}}{2}$$

$$C_{44}' = C_{55}' = \frac{C_{44} + C_{55}}{2}$$

$$C_{33}' = C_{33}$$

$$C_{66}' = C_{66}$$

$$C_{41}' = C_{52}' = d_x' C_{11}'$$

$$d_{xy}' = d_{xy}$$

$$C_{63}' = -d_{xy} C_{33}' \qquad (16)$$

Let the Poisson's Ratio be the average of the orthotropic values defined in Reference 3.

$$\nu' = \frac{\nu_{xy} + \nu_{yx}}{2}$$

$$C_{21}' = \nu' C_{11}'$$

$$C_{15}' = C_{21}' d_y'$$

$$C_{45}' = C_{45}$$

*The primed quantities represent the square end trays

TABLE 3. TRAY PANEL EFFECTIVE ORTHOTROPIC PROPERTIES

Type	t_x cm	t_y cm	t_{xy} cm	d_x cm	d_y cm	d_{xy} cm	ν_{yx}	ν_{xy}
Side Trays								
Debris	.0493	.0112	.0211	9.096	9.627	4.049	-.116	-.512
Shallow	.0500	.0109	.0142	9.174	9.716	4.016	-.118	-.538
Nominal	.0950	.0282	.0254	9.136	9.474	-1.199	-.105	-.351
Deep	.100	.0323	.0188	9.098	9.558	-25.077	-.111	-.344
End Trays								
Rectangular								
Shallow	.104	.121	.0254	7.836	7.859	1.803	-.0742	-.0641
Nominal	.113	.129	.0198	7.922	7.963	.305	-.0461	-.0404
Deep	.121	.136	.0145	7.996	8.057	-2.316	-.0217	-.0193
Square								
Shallow	.113	.113	.0254	7.849	7.849	1.803	-.0692	-.0692
Nominal	.121	.121	.0198	7.943	7.943	.305	-.0433	-.0433
Deep	.129	.129	.0145	8.026	8.026	-2.316	-.0205	-.0205

STATIC TEST - ANALYSIS EVALUATION OF ATTACHMENTS

Static test data was used to evaluate the SPAR model longeron-to-intercostal joint condition and the diagonal end-fitting flexibility. The two types of static tests that were performed are shown in Figure 24. The SPAR static deflections are shown as a percent of the test deflections for both the bending and torsion tests. The model and tests were performed on the LDEF configurations without trays. The ball and pin joints refers to the longeron-to-intercostal joints previously discussed and shown in Figures 5, 12, and 13. From this information it was decided to perform first the dynamic analysis without trays, using the model that included the diagonal end flexibility. The pin joint model was considered to be the intent of the longeron-to-intercostal joint design. However, it was observed that there was some out of plane motion because of the tolerance in the clevis joints that led to the consideration of modeling using ball joints. The true joint condition is someplace between these two. For the dynamic analysis without trays, it was decided to evaluate both the ball joint and pin joint conditions for comparison because the static test deflection correlation with analysis was not conclusive.

LDEF Configuration Without Trays

Bending

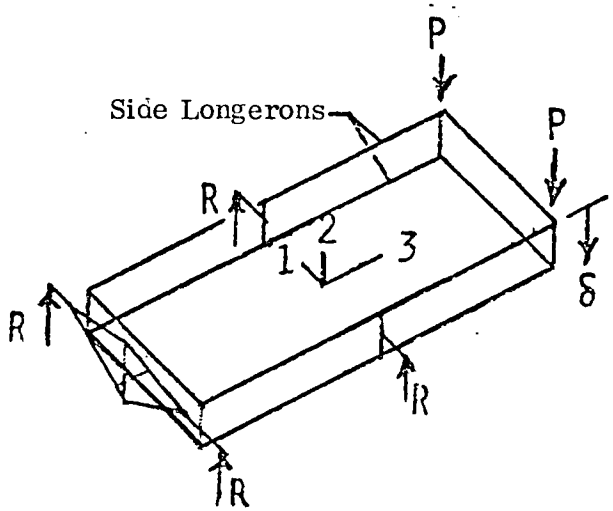

Torsion

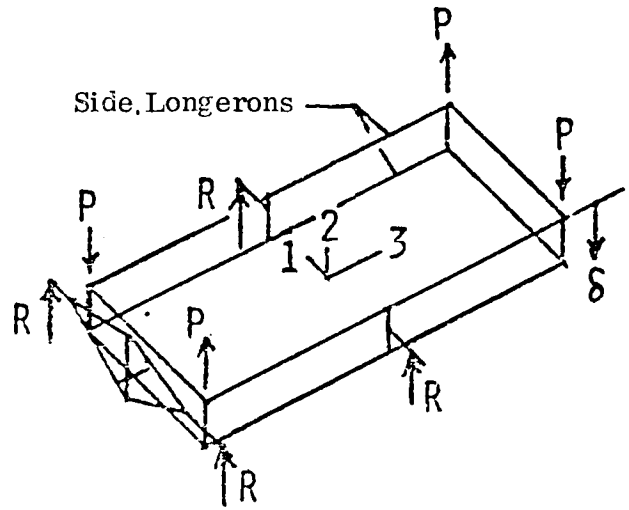

	Without End** Flexibility (%)	With End** Flexibility (%)	Without End** Flexibility (%)	With End** Flexibility (%)
Ball* Joints	77.7	99.7	94.4	110.6
Pin* Joints	71.1	89.6	75.6	84.8

$$\text{Percent} = \frac{\text{SPAR deflection}}{\text{test deflection}} \times 100$$

*Longeron-to-Intercostal Joints

**End Flexibility Refers to the Diagonal-to-Center Bhd Flat Plate Fittings

Figure 24. Analytical and Measured Static Deflections

MASS PROPERTIES

As previously discussed in the section on the SPAR LDEF model, the model was divided into nine substructure groups as shown in Table 1. For each SPAR group in Table 1, the consistent mass matrix is generated by SPAR and the weight of each group is printed out. Table 4 shows the weight of eight of the nine groups representing the weight of the SPAR model without trays before the diagonal end flexibility beam elements were added. All of the groups had E21 beam elements and the IECM shelf also had E43 panel elements. The total SPAR weight at the group level was compared with the drawing weight and the lumped masses in SPAR were adjusted at the group level for better agreement with the drawing weight. This procedure results in an accurate overall weight distribution control. The total SPAR weight without trays is 3648 kg (8041 pounds). The keel pin and the damper weights are not included in this model or the test configuration. This model weight was 0.2% lighter than the weight statement. The final lumped masses and grid point locations for the final configuration with trays are tabulated in Table 5. Most of these weights are the end fitting weights and miscellaneous hardware. Table 6 shows SPAR weight distribution for the final configuration with trays. The total SPAR tray weights, 5218.1 kg (11504 pounds), exactly equals the test configuration and includes the weight of the trays, the base plates and the dummy weights that were bolted to the base plate. These total weights for each tray are tabulated in Figure 21. The total with tray SPAR model weight was 9057 kg (19967 pounds).

The total weight for each tray was distributed uniformly over the surface of the effective panel area. The radial location of the tray and base plate center of gravity is based on SPAR weight outputs of the static tray models. The effective panel area of bays A, B, E and F was 1.4921m^2 (2312.7 in^2). The two center bays C and D had an effective panel area of 1.6197 m^2 (2510.6 in^2). The mass moments of inertia of each tray due to the radial offset of each tray center of gravity from the plane of the four corner longeron grid points was determined and one fourth was applied to each of the four corner grid points as shown in Appendix C.

TABLE 4. SPAR GROUPING FOR WEIGHT BALANCE, CONFIGURATION WITHOUT TRAYS

SPAR Type	Group Number	Title	SPAR Weight (kg)	Lumped Mass (kg)	Total SPAR (kg)	Drawing Weight (kg)
E21	1	Longeron	910.3	189.1	1099.4	1082.6
E21	2	Intercostals	355.9	0.0	355.9	366.7
E21	3	Center Bhd.	639.5	278.7	918.2	945.6
E21	4	Forward Bhd.	188.8	64.0	252.8	257.0
E21	5	Aft Bhd.	188.8	64.0	252.8	257.0
E21	6	Diagonals	279.0	154.7	433.7	433.8
E21	7	Cross Beam	94.2	75.3	169.5	169.4
E21	8	IECM Shelf	16.6	4.5	26.3	26.2
E43	1	IECM Shelf	5.2			
	Sub Total		2678.3	830.3	3508.6	3508.3
Misc. Hardware (on Bhds.)			—	55.2	55.2	55.2
2 Trunnion Instl. (on Center Bhd.)			—	56.5	56.5	57.3
Spindle Pin Instl. (Fwd. Bhd.)			—	19.8	19.8	19.8
80 Clips (Fwd. and Aft Bhd.)			—	7.4	7.4	7.4
			2678.3	969.2	3647.5	3648.0

TABLE 5. LUMPED MASS LOCATIONS, CONFIGURATION WITH TRAYS

Grid Point	Mass (kg)	Grid Point	Mass (kg)
1	26.08	79	30.37
5	26.08	80	30.16
9	32.99	81	22.01
10	15.32	82	34.61
11	.66	83	78.24
12	.66	84	50.07
13	.66	87	50.07
14	.66	88	78.24
15	15.32	99	2.25
16	15.32	100	2.25
17	.66	149	15.32
18	.66	150	.66
19	.66	151	.66
20	.66	152	.66
21	15.32	153	.66
22	1.65	154	15.32
23	1.65	155	15.32
24	1.65	156	.66
27	1.65	157	.66
28	115.43	158	.66
29	1.65	159	.66
32	1.65	160	15.32
33	1.65	161	1.65
34	1.65	162	1.65
71	34.61	163	1.65
72	22.01	166	1.65
73	30.16	167	1.65
74	30.37	170	1.65
75	22.01	171	1.65
76	34.61	172	1.65
77	34.61	181	133.24
78	22.01		
		Total	1102.00
			(2429.5 lb)

TABLE 6. SPAR WEIGHT, CONFIGURATION WITH TRAYS

	SPAR Weight (kg)	Lumped Mass (kg)	Total SPAR (kg)
Longerons	910.3	189.1	1099.4
Intercostals	355.9	0.0	355.9
Center Bhd.	639.5	278.6	918.1
Fwd. Bhd.	188.8	64.0	252.8
Aft Bhd.	188.8	64.0	252.8
Diagonals	315.8	154.7	470.5
Cross Beam	116.1	75.3	191.4
IECM Shelf	21.7	4.5	26.2
Miscellaneous	——	271.8	271.8
Total Without Trays	2736.9	1102.0	2828.9
Trays	5218.1	0.0	5218.1
Total	7955.0	1102.0	9057.0

COMPARISON OF FREQUENCIES AND MODE SHAPES

Configuration Without Trays

The comparison of some of the SPAR and test vibration modes is shown in Figure 25 for the LDEF without trays. The ball-joint and pin-joint analyses bracket the test data at the lower LDEF frequencies. In general, the longeron-to-intercostal ball joint boundary condition was closer to the test data so this boundary condition was selected for the vibration analysis with trays. Analytical frequencies were higher than test for the second vertical and lateral bending modes. There were many intermediate modes not shown, especially in the 16 to 30 Hertz range where the predominate response was diagonal motion often coupled with longeron lateral motion.

The first SPAR lateral bending mode shape at 20.85 Hertz is compared with the test mode at 21.38 Hertz in Figure 26. The dashed lines represent the undeformed test shape. The straight solid longeron lines are those that had no transducers in the test. By comparing the shape of individual longerons and diagonals, reasonable mode shape comparisons exist. The first SPAR vertical bending mode shape at 28.39 Hertz is compared with the mirror image of the test mode at 28.52 Hertz in Figure 27. Again the individual longeron and diagonal mode shapes compare. Figure 28 shows the first SPAR torsion mode at 12.94 Hertz compared with Figure 29 showing the test mode at 14.14 Hertz.

Configuration With Trays

The LDEF configuration with trays was evaluated using the longeron-to-intercostal ball joint SPAR model. Figure 30 shows the comparison of a few SPAR and test modes of LDEF with trays. The SPAR and test frequencies of the first three fundamental LDEF modes had very close correlation considering the complexity of the variation in trays and the longeron-to-intercostal joint motions.

Frequency, Hz			Mode Description
SPAR		Test	
Ball Joints	Pin Joints		
5.90	5.90	6.55	Cross Beam Rigid Body Yaw
9.41	9.41	10.14	Cross Beam Longitudinal Bending
12.94	15.90	14.14	First Torsion
20.85	22.29	21.38	First Lateral Bending
16.2 to 28.9	17.7 to 30.0	19 to 26	Predominantly Diagonal Motion
28.39	30.15	28.52	First Vertical Bending
28.86	31.60	29.28	Second Torsion
38.86	40.23	33.37	Second Vertical Bending
40.78	41.26	34.51 35.36	Second Lateral Bending

Figure 25. LDEF SPAR and Test Vibration Modes Without Trays

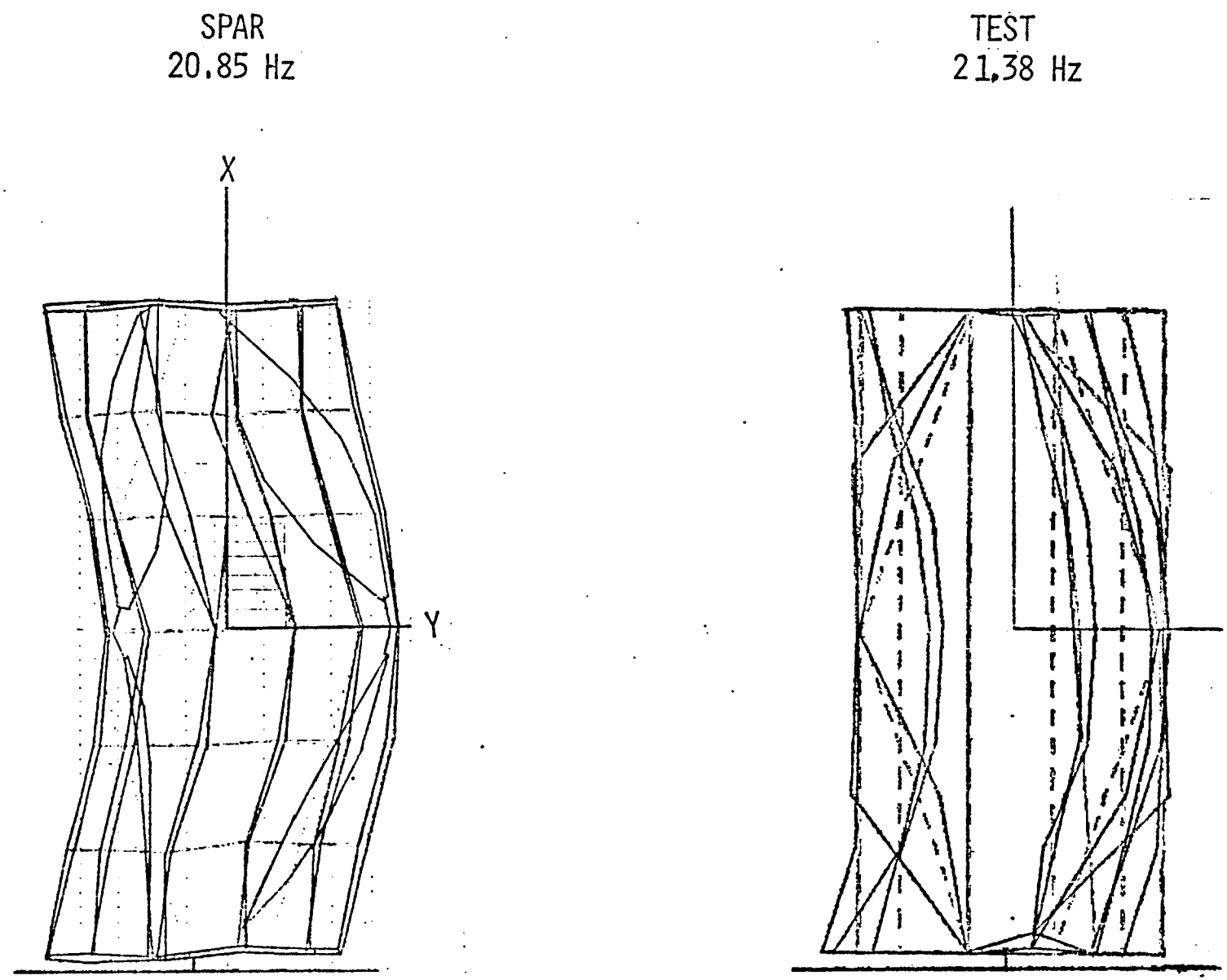

Figure 26. First Lateral Bending Mode Without Trays

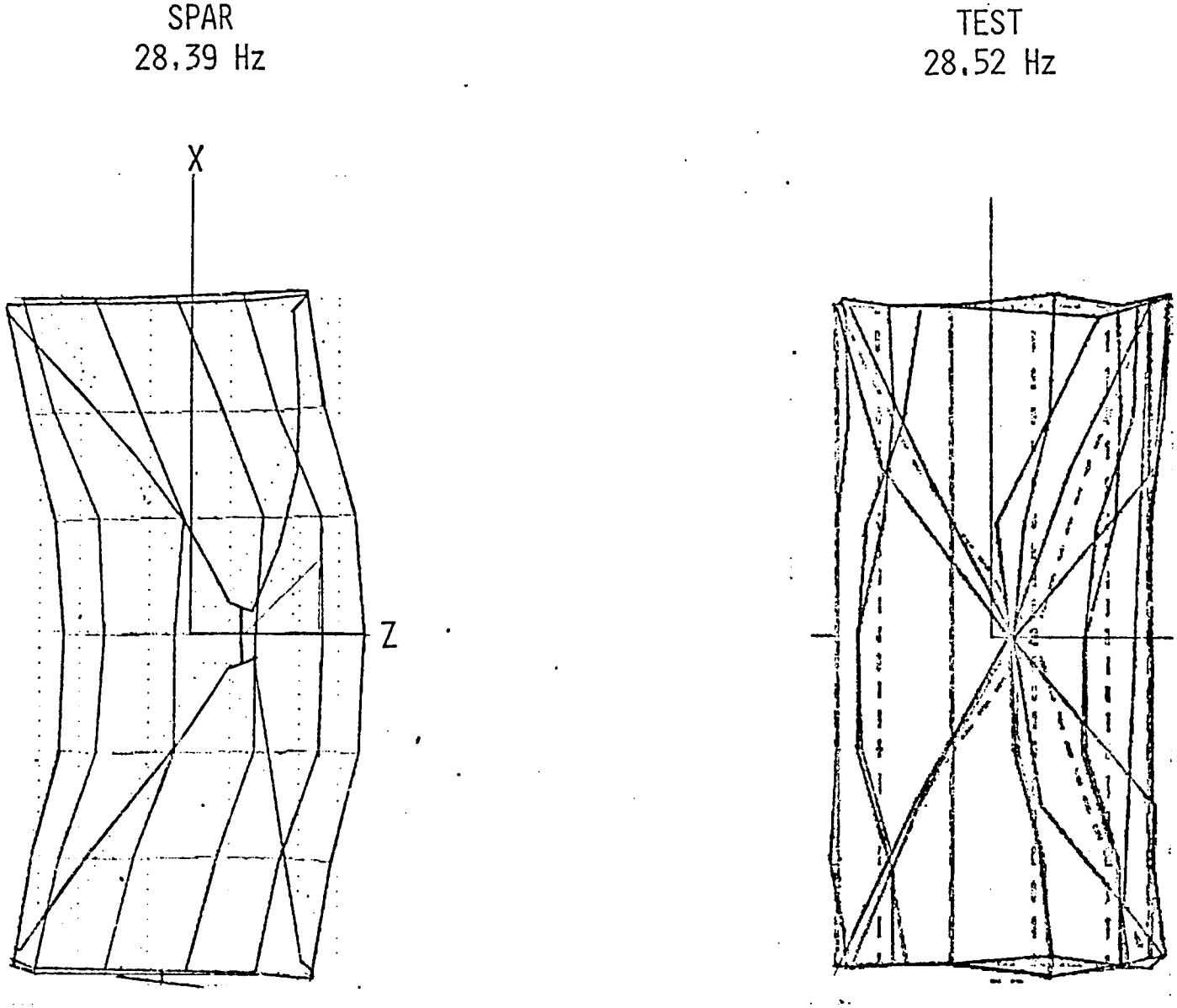

Figure 27. First Vertical Bending Mode Without Trays

SPAR
12.94 Hz

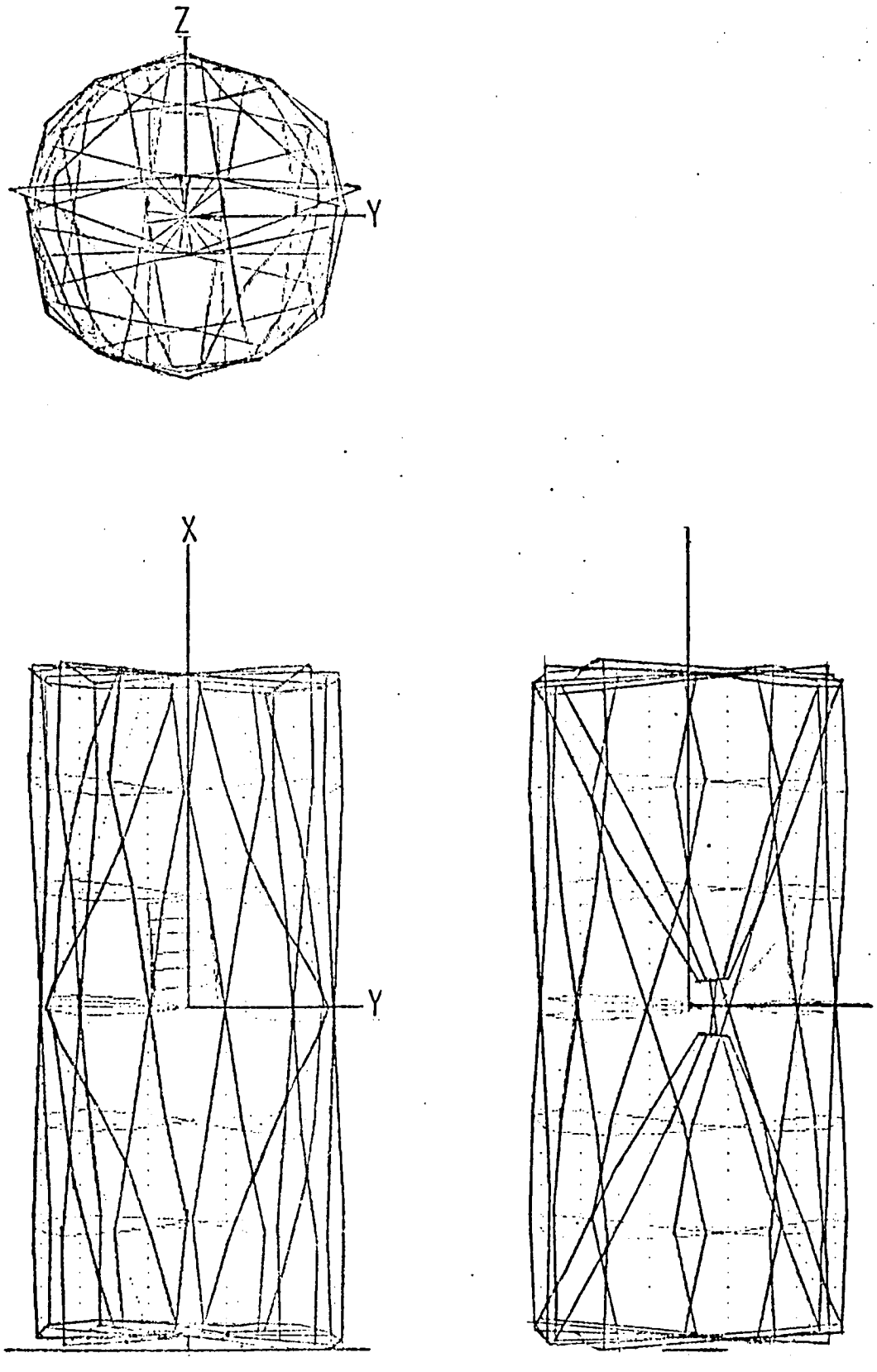

Figure 28. First SPAR Torsion Mode Without Trays

TEST
14.14 Hz

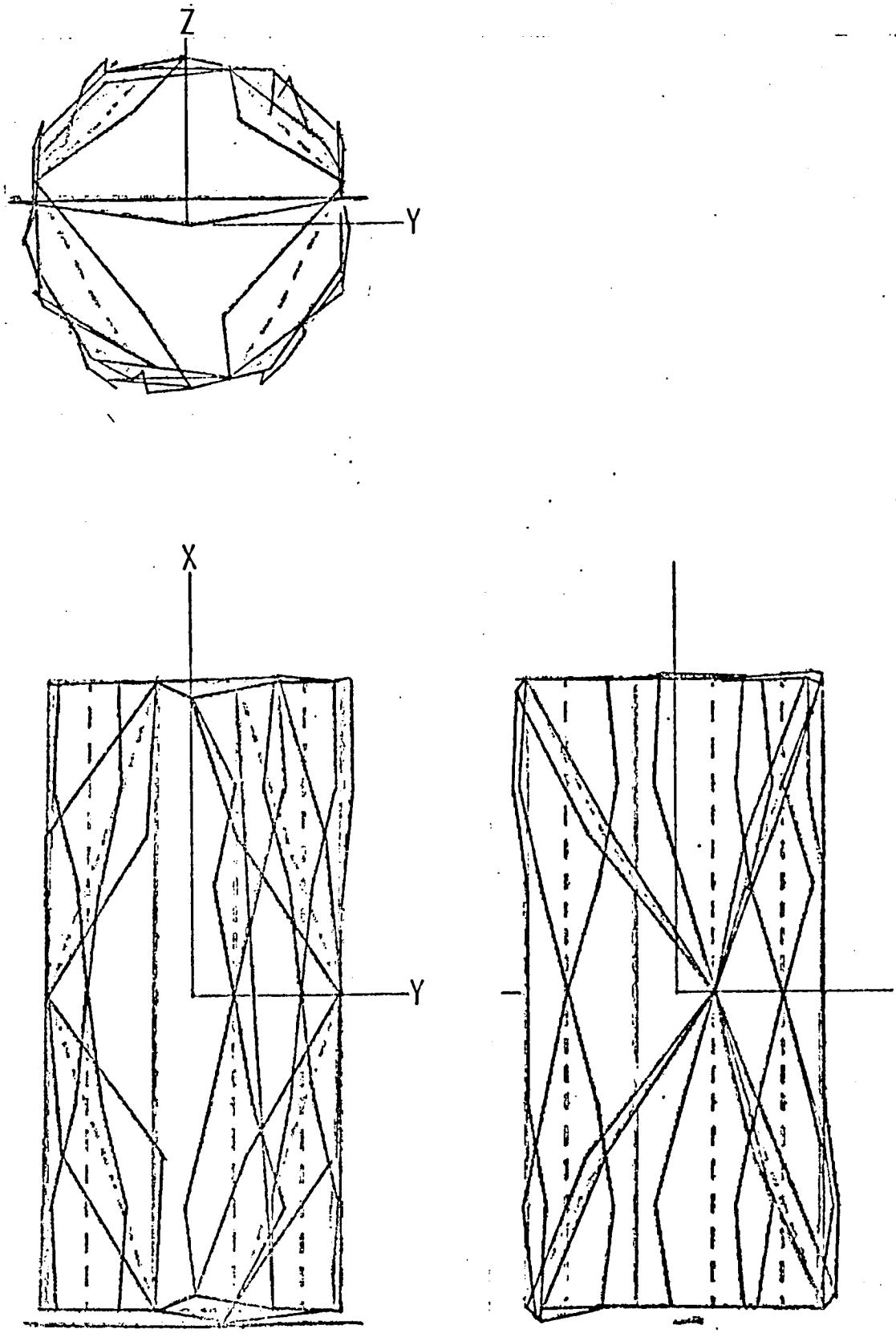

Figure 29. First Test Torsion Mode Without Trays

(Longeron to Intercostal Ball Joints)

Frequency, Hz		Mode Description
SPAR	Test	
5.72	6.10	Cross Beam Rigid Body Yaw
9.33	10.10	Cross Beam Longitudinal Bending
19.06	19.20	1st Torsion
22.75	21.83	1st Lateral Bending
25.74	23.90	1st Vertical Bending

Figure 30. SPAR and Test Modes With Trays

REMARKS AND CONCLUSIONS

The LDEF structure presented some unique features to challenge the finite element modeling techniques.

1. The design of the longeron-to-intercostal clevis pin joint modified the LDEF bending stiffness and torsional stiffness. Static bending and torsional test data of the LDEF vehicle without trays installed was valuable in assessing this joint boundary condition. The ball-joint boundary condition was selected as more accurate than the pin-joint boundary condition based on this static test data and by comparing the vibration analysis of the two boundary conditions with vibration test data of the LDEF configuration without trays.

2. The design of the diagonal end fitting that connected two diagonals to a common point on the center bulkhead was a tee shaped flat plate. This fitting appeared to be stiff enough so that it could be treated as a rigid link. However, there was a slight angle offset between the diagonal and the plane of the end fitting so that axial loads in the diagonal resulted in bending and twisting of this fitting. Again, the static bending and torsional test data was found to be valuable in determining that the flexibility of this diagonal end fitting was required.

3. The design of the tray-to-structure clamps shown in Figures 7 and 8 allowed in plane relative sliding motion between the tray flange and the mounting structure. At the four side mid point clamps this relative sliding motion was approximated in the tray effective panel stiffness matrix by allowing degree of freedom 6 to be free when the tray finite element model was subjected to static shear and twisting deformations. This boundary change reduced the shear stiffness to 54 percent and twisting stiffness to 58 percent of the shear and twisting stiffnesses for the original boundary condition.

4. Using the SPAR LDEF model and incorporating the modeling features described above resulted in good agreement between analytical and measured data. This was true for static deflections and vibrations modes.

APPENDIX A

PANEL AND BEAM PROPERTIES

TRAY PANEL STIFFNESS

Effect of Boundary Conditions on Tray Panel Stiffness

After examing the clamping conditions of the tray lip to the mounting structure it was decided to allow some clamp sliding due to shear loading. As shown in Figure 8, the clamp friction is the only restraint for relative in-plane motion, since there are no through bolts. The 4 clamps at the center of each side of the tray were allowed to slide parallel to the edge of the tray to relieve some of the shear loads being transferred at these clamp locations. No sliding was allowed at the 4 corner clamp locations. By freeing the degree of freedom 6 boundary condition at the ends of four rigid links as shown below in the right hand column, it was determined that the total shear transfer per side was reduced to approximately one half when the unity shear strain loading conditions were applied. The Debris tray stiffness matrix was derived with and without the relaxed boundary condition being used for the unit shear and unit twist cases. The numerical comparison is shown in Table 7. The shear and twisting stiffness terms were approximately one half as stiff with the relaxed boundary condition. This relaxed boundary condition was used for the derivation of all of the effective panel stiffness terms with the values tabulated in Table 8.

	Original Boundary (No Relative Tray Lip Motion)	Relaxed Boundary (With Relative Tray Lip Motion) (See Table 2)
Grid Point No.	θ_z	θ_z
1	0	0
2	0	Free
3	0	0
4	0	0
5	0	Free
6	0	0
7	0	Free
8	0	Free

SPAR BEAM SECTION PROPERTIES

The SPAR beam configurations and section properties are tabulated in Table 9. The locations of these beam elements in the SPAR model are indicated in Figures 11, 14 and 19.

TABLE 7. FLANGE ROTATION EFFECT ON DEBRIS PANEL STIFFNESS MATRIX

Relative Flange Motion Allowed (θ_z = Free)

$$\begin{Bmatrix} N_x \\ N_y \\ N_{xy} \\ M_x \\ M_y \\ M_{xy} \end{Bmatrix} = \begin{bmatrix} .3604 & -.04186 & 0 & 3.278 & -.3314 & 0 \\ -.04186 & .08170 & 0 & -.2702 & .7864 & 0 \\ 0 & 0 & .05594 & 0 & 0 & -.2264 \\ 3.278 & -.2702 & 0 & .2564 & -.01664 & 0 \\ -.3314 & .7864 & 0 & -.01664 & .07187 & 0 \\ 0 & 0 & -.2264 & 0 & 0 & .009610 \end{bmatrix} \begin{Bmatrix} e_x \\ e_y \\ e_{xy} \\ k_x \\ k_y \\ k_{xy} \end{Bmatrix}$$

Relative Flange Motion Not Allowed ($\theta_z = 0$)

$$\begin{Bmatrix} N_x \\ N_y \\ N_{xy} \\ M_x \\ M_y \\ M_{xy} \end{Bmatrix} = \begin{bmatrix} .3604 & -.04186 & 0 & 3.278 & -.3314 & 0 \\ -.04186 & .08170 & 0 & -.2702 & .7864 & 0 \\ 0 & 0 & .1034 & 0 & 0 & -.4059 \\ 3.278 & -.2702 & 0 & .2564 & -.01664 & 0 \\ -.3314 & .7864 & 0 & -.01664 & .07187 & 0 \\ 0 & 0 & -.4059 & 0 & 0 & .01655 \end{bmatrix} \begin{Bmatrix} e_x \\ e_y \\ e_{xy} \\ k_x \\ k_y \\ k_{xy} \end{Bmatrix}$$

where the units are

$$[C] = \left[\begin{array}{c|c} \text{MN/cm} & \text{MN} \\ \hline \text{MN} & \text{Mm-N} \end{array}\right]$$

The only stiffness terms that change are the C_{33}, C_{36}, C_{63} and C_{66} terms. By allowing the flange motion the shear stiffness, C_{33}, reduced from .1034 to .05594 or only 54.1 percent as stiff. The twisting stiffness, C_{66}, reduced to 58.1 percent and the coupling term, C_{36}, reduced to 55.8 percent as stiff.

TABLE 8. TRAY PANEL STIFFNESS TERMS
(Side Flanges Free to Rotate)

	C_{11} MN/cm	C_{12} (MN/cm)	C_{22} (MN/cm)	C_{33} (MN/cm)	C_{14} (MN)	C_{15} (MN)	C_{24} (MN)
Side Trays							
Debris	.3604	-.04186	.08170	.05594	3.278	-.3314	-.2072
Shallow	.3690	-.04361	.08105	.03748	3.386	-.3616	-.2943
Nominal	.6805	-.07112	.20245	.06772	6.217	-.5654	-.3527
Deep	.7192	-.07972	.2319	.04963	6.544	-.5712	-.3671
End Rectangular							
Shallow	.7234	-.05368	.8375	.06713	5.669	.03661	.00934
Nominal	.7788	-.03590	.8877	.05277	6.169	.08776	.06107
Deep	.8341	-.01813	.9380	.03841	6.669	.1389	.1128
End Corner							
Shallow	.7805	-.05401	.7805	.06713	4.448	-.4261	-.4261
Nominal	.8333	-.03604	.8333	.05277	6.618	-.2862	-.2862
Deep	.8861	-.01816	.8861	.03841	7.113	-.1458	-.1458

	C_{25} (MN)	C_{36} (MN)	C_{44} (Mm-N)	C_{45} (Mm-N)	C_{55} (Mm-N)	C_{66} (Mm-N)
Side Trays						
Debris	.7864	-.2264	.2564	-.01664	.07187	.009610
Shallow	.7873	-.1505	.2678	-.02001	.07249	.006602
Nominal	1.918	.08118	.3868	-.01580	.1655	.003100
Deep	2.216	1.2446	.3480	.00264	.1866	.02307
End Rectangular						
Shallow	6.582	-.1210	.4365	.01427	.5481	.004519
Nominal	7.069	-.01606	.4802	.01271	.5922	.009850
Deep	7.556	.08892	.5232	.01115	.6363	.02106
End Corner						
Shallow	6.126	-.1210	.4923	.01427	.4923	.004519
Nominal	6.618	-.01606	.5362	.01271	.5362	.009850
Deep	7.113	.08892	.5797	.01115	.5797	.02106

TABLE 9. SPAR SECTION PROPERTIES

Beam Elements

SPAR Beam Section Property	SPAR Designation	B1 (cm)	T1 (cm)	B2 (cm)	T2 (cm)	B3 (cm)	T3 (cm)	Area (cm^2)	I_1 (cm^4)	I_2 (cm^4)	J (cm^4)
BA1	WFL	11.43	.9652	15.8496	.5588	-	-	30.92	240.4	1746.7	7.8
BA2	TEE	11.43	.9652	7.6708	.5588	-	-	15.32	120.2	79.4	3.8
BA3	WFL	17.78	1.4732	83.1514	.9144	-	-	77.56	1381.8	12619.7	44.9
BA4	WFL	11.43	.9652	22.1996	.5588	-	-	34.47	240.5	3471.2	8.1
BA5	GIVN	35.56	1.270	25.40	.635	8.89	1.016	129.03	12444.1	17975.4	8495.3
BA6	WFL	10.16	.762	13.716	.4572	-	-	21.75	133.3	910.5	3.4
BA7	GIVN	26.518	.3556	15.24	.4572	3.7338	.762	42.78	3788.6	1940.5	2080.6
BA8	TUBE	6.985	7.620	-	-	-	-	29.14	778.3	778.3	1556.6
BA9	TUBE	3.81	5.08	-	-	-	-	35.47	357.6	357.6	715.1
BA10	GIVN	38.10	1.5748	12.70	1.27	22.86	2.54	116.52	10570.2	877.8	1216.6
BA11	GIVN	5.08	3.302	8.636	.762	2.54	.508	32.52	119.3	426.5	63.7
BA12	CHN	4.445	.6604	6.2992	.4318	-	-	8.59	80.3	17.2	1.0
BA13	ANG	2.235	.1600	2.380	.1600	-	-	0.74	0.7	0.2	0.01
BA14	TUBE	2.416	2.54	-	-	-	-	1.94	6.0	6.0	11.9
BA15	TUBE	.254	6.9088	-	-	-	-	149.75	1789.4	1789.4	3578.7
BA16	GIVN	(Same as BA2 for Ball Joints)				-	-	15.32	0	0	0
BA18	GIVN	(Same as BA2 for Pin Joints)				-	-	15.32	120.2	0	3.8
BA19	GIVN	18.288	2.54	-	-	-	-	46.45	1294.6	25.0	99.9
BA20	GIVN	17.78	1.905	-	-	-	-	33.87	892.3	10.2	41.0

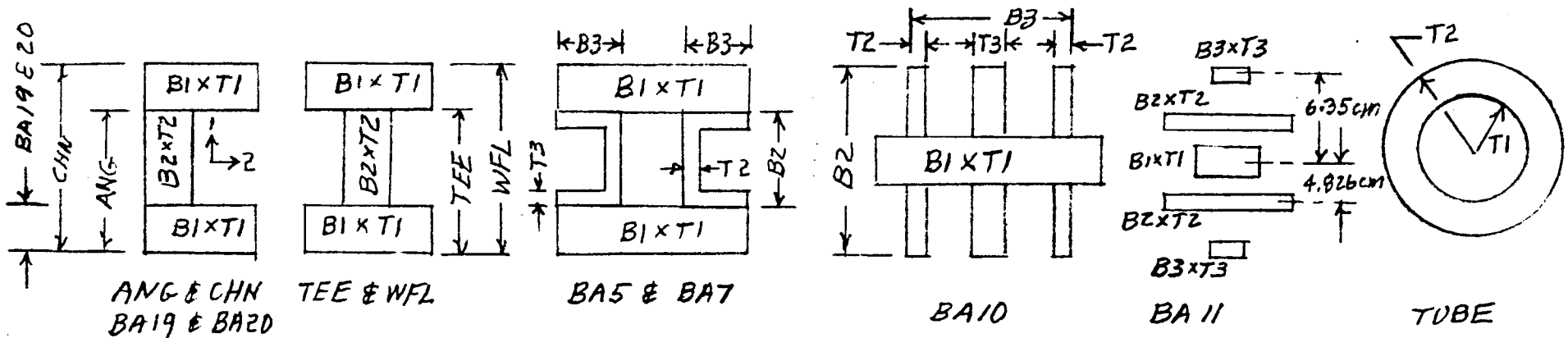

SA1

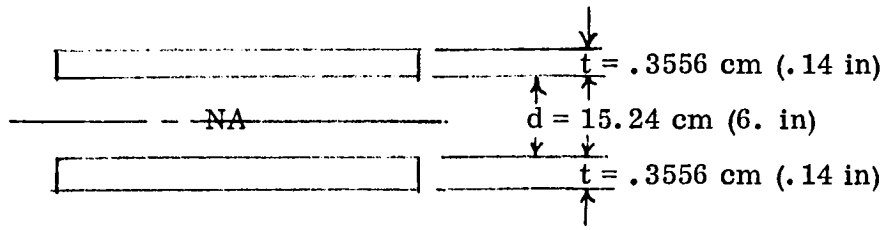

The bending stiffness for a single panel is:

$$D = \frac{Eh^3}{12\,(1-\nu^2)}$$

This bending stiffness was derived in Reference 2 from the integration

$$M = \int_{-h/2}^{h/2} \sigma_x\, z\, d\, z$$

For a two plate configuration the integration is

$$M = \int_{-d/2\ -t}^{-d/2} \sigma_x\, z\, d\, z + \int_{d/2}^{d/2+t} \sigma_x\, z\, d\, z$$

resulting in the bending stiffness

$$D' = \frac{Et}{(1-\nu^2)}\left(\frac{1}{2}d^2 + dt + \frac{2}{3}t^2\right)$$

SPAR FORMAT = 2 inputs

$$\begin{Bmatrix} N_1 \\ N_2 \\ N_{12} \end{Bmatrix} = \begin{bmatrix} 2\frac{Et}{(1-\nu^2)} & 2\frac{\nu Et}{(1-\nu^2)} & 0 \\ 2\frac{\nu Et}{(1-\nu^2)} & 2\frac{Et}{(1-\nu^2)} & 0 \\ 0 & 0 & \frac{Et}{(1+\nu)} \end{bmatrix} \begin{Bmatrix} e_x \\ e_y \\ e_{xy} \end{Bmatrix}$$

$$\begin{Bmatrix} M_1 \\ M_2 \\ M_{12} \end{Bmatrix} = \begin{bmatrix} D' & \nu D' & 0 \\ \nu D' & D' & 0 \\ 0 & 0 & \frac{D'(1-\nu)}{2} \end{bmatrix} \begin{Bmatrix} k_x \\ k_y \\ k_{xy} \end{Bmatrix}$$

SA2

.160 cm (.063 in.)

Plate element having extensional, bending and shear stiffness

APPENDIX B

MESH SIZE CRITERION

MESH SIZE CRITERION

Maximum finite element grid intervals or mesh sizes were determined by use of a criterion stating that a beam or plate element having simply supported boundary conditions should have a natural frequency greater than 50 Hertz. If the natural frequency was less than 50 Hertz, intermediate grid points were added until the criterion was met. The value of 50 Hertz was selected because the region of LDEF frequencies of interest were those up to 50 Hertz. As shown in Figure 31, the only place that intermediate grid points were required was on the diagonals and lateral members of the cross beam.

Required: Frequency > 50 Hz

Boundary Condition: Simply Supported

Beam Elements

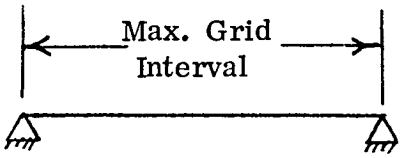

Met Criteria	Failed Criteria
(> 50 Hz)	(< 50 Hz) (Intermediate grid points added)
Longerons	Diagonals
Intercostals	Cross beam - lateral elements
Bulkheads	
IECM Shelf	
Cross beam - vertical center element	

Plate Elements

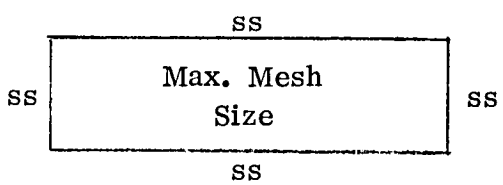

Met Criteria

(> 50 Hz)

All plate elements met the criteria

Figure 31. Mesh Size Criterion

APPENDIX C

TRAY MASS MOMENTS OF INERTIA

TRAY MASS MOMENTS OF INERTIA

The mass moment of inertia of a given tray type (I_t) was obtained from the SPAR tray substructure group weights and the radial offset distance ($\bar{z}_t$) to the tray mass center from the plane of the corner longeron grid points. These values are tabulated in Table 10.

$$\bar{z} = \frac{\Sigma wz}{\Sigma w}$$

$$I_t = \bar{z}^2 \Sigma w$$

The average ballast height for each tray and the total ballast weight (w_b) for each tray was used to determine the ballast offset distance ($\bar{z}_b$) and the ballast mass moment of inertia (I_b). These values are tabulated in Table 11.

$$I_b = \bar{z}_b^2 w_b$$

The total tray radial offset mass moment of inertia for each tray is

$$I = I_t + I_b$$

One fourth of this value was then applied at each of the four corner grid points and rotated from the tray coordinate system to the LDEF cylindrical coordinate system.

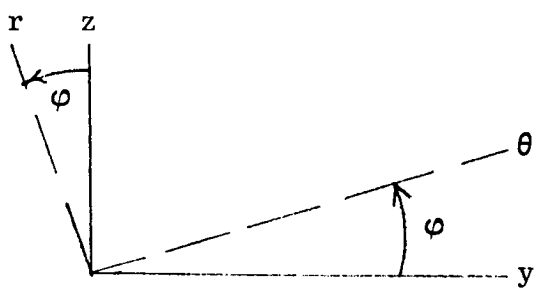

x, y, z Tray coordinates

r, θ, z' LDEF coordinates

Mass Moments of Inertia in LDEF Coordinates

$$I_\theta = I_y \cos^2 \varphi + I_z \sin^2 \varphi - 2 I_{yz} \sin \varphi \cos \varphi$$

$$I_r = I_y \sin^2 \varphi + I_z \cos^2 \varphi + 2 I_{yz} \sin \varphi \cos \varphi$$

$$I_{\theta r} = I_{yz} \cos 2\varphi + \frac{1}{2} (I_y - I_z) \sin 2\varphi$$

For $I_y = I/4$; $I_z = I_{yz} = 0.0$

$$I_\theta = (I/4) \cos^2 \varphi$$

$$I_r = (I/4) \sin^2 \varphi$$

$$I_{r\theta} = (I/8) \sin^2 \varphi$$

$$I_{z'} = I/4$$

$$\varphi = \pm 15^o$$

$$\cos^2 \varphi = .93301$$

$$\sin^2 \varphi = .06699$$

TABLE 10. SUMMARY OF SIDE TRAY OFFSETS AND MASS MOMENTS OF INERTIA

Tray Type	Tray and Base Plate Mass, kg (lb)	$\bar{z}_t$ Tray Mass Offset, cm(in)	I_t, m^2-kg (in-lb-sec^2)
Debris	24.05 (53.023)	2.78 (1.096)	.01863 (.1648)
Shallow	26.09 (57.519)	2.35 (.925)	.01443 (.1276)
Nominal	29.00 (63.937)	-3.53 (-1.390)	.03614 (.3196)
Deep	32.24 (71.083)	-9.01 (-3.547)	.2619 (2.316)
Deep*	48.14 (106.137)	-40.4 (-15.9)	7.847 (69.40)

*Special deep tray at location D-12

TABLE 11. SIDE TRAY BALLAST MASS MOMENTS OF INERTIA

Tray Location	Ballast Weight (kg)	$\bar{z}_b$ Ballast Offset (cm)	I_b (m^2-kg)	Tray Location	Ballast Weight (kg)	$\bar{z}_b$ Ballast Offset (cm)	I_b (m^2-kg)
A-1	0	-	0	D-1	73.94	4.902	.1777
A-2	70.31	-3.037	.06486	D-2	0	-	0
A-3	51.71	4.318	.09643	D-3	0	-	0
A-4	68.04	-3.037	.06278	D-4	73.94	4.902	.1777
A-5	0	-	0	D-5	0	-	0
A-6	0	-	0	D-6	70.31	-3.037	.06486
A-7	16.33	2.945	.01416	D-7	0	-	0
A-8	0	-	0	D-8	74.84	4.903	.1799
A-9	70.31	-3.037	.06486	D-9	0	-	0
A-10	70.31	-3.037	.06486	D-10	27.22	3.326	.03012
A-11	0	-	0	D-11	73.94	4.902	.1777
A-12	38.56	3.835	.05672	D-12	131.09	-49.530	32.159
B-1	0	-	0	E-1	16.33	2.945	.01416
B-2	68.04	-10.659	.7730	E-2	68.04	-10.659	.7730
B-3	70.31	-3.037	.06486	E-3	65.32	4.901	.1569
B-4	8.16	3.254	.00864	E-4	70.31	-3.037	.06486
B-5	68.04	-10.659	.7730	E-5	68.04	-10.659	.7730
B-6	13.15	3.125	.01284	E-6	28.12	3.327	.03112
B-7	68.04	-10.659	.7730	E-7	68.04	-10.659	.7730
B-8	8.16	3.254	.00864	E-8	70.31	-3.037	.06486
B-9	70.31	4.903	.1690	E-9	70.31	-3.037	.06486
B-10	31.75	-12.182	.4712	E-10	68.04	-10.659	.7730
B-11	0	-	0	E-11	0	-	0
B-12	8.16	3.254	.00864	E-12	10.43	-12.616	.1660
C-1	8.16	3.254	.00864	F-1	16.33	2.945	.01416
C-2	0	-	0	F-2	11.79	2.996	.01058
C-3	26.76	3.250	.02827	F-3	37.19	-4.181	.06500
C-4	27.22	3.326	.03012	F-4	0	-	0
C-5	42.18	3.887	.06373	F-5	11.79	2.996	.01058
C-6	70.31	-3.037	.06486	F-6	10.43	-4.946	.02551
C-7	0	-	0	F-7	0	-	0
C-8	73.94	4.902	.1777	F-8	44.00	3.886	.06644
C-9	21.77	3.125	.02126	F-9	37.19	-4.181	.06500
C-10	8.16	3.254	.00864	F-10	0	-	0
C-11	73.94	4.902	.1777	F-11	0	-	0
C-12	33.57	3.632	.04428	F-12	44.91	-4.054	.07382

APPENDIX D

SPAR EIGENVALUE EXTRACTION

EXPERIENCE

SPAR EIGENVALUE EXTRACTION EXPERIENCE

Vibration modes are computed in SPAR by means of a sparse matrix eigensolver as described in reference 1. The procedure implements an iterative process consisting of a Stodola (matrix iteration) procedure followed by a Rayleigh-Ritz procedure, followed by a second Stodola procedure, etc., resulting in successively refined approximations of a reduced set of m eigenvalues. Since K need not be positive definite, this method can be used to solve "shifted" vibration eigenproblems. This "shifted" procedure is required for a free-free system to make the stiffness matrix non-singular. The procedure used in SPAR is to alter the original linear vibration problem

$$r\,Mx - Kx = 0 \tag{1}$$

by adding and subtracting cMx from the left side,

$$(r - c)\,Mx - (K - cM)\,x = 0 \tag{2}$$

Equation 2 is of the same form as equation 1, except that (r - c) has replaced r, and (K - cM) has replaced K. The value c is the shift value. SPAR inverts the shifted stiffness matrix (K - cM) and computes the eigenvalues in the neighborhood of c. When this inversion is being made, the number of negative terms encountered in factoring K - cM is equal to the number of roots (eigenvalues) below the shift value (c) in equation (2).

Using this SPAR procedure for the LDEF model without trays required eleven computer runs to obtain all of the flexible modes up to 50 Hertz as illustrated in Figure 32. The inputs shown for each computer run are the upper and lower frequency bounds (V1 and V2) and the shift location indicated by the triangle. The outputs shown are the number of converged eigenvalues and the frequency range of these converged eigenvalues. The first run is shown on the bottom right of the figure with a shift at 50 Hertz and the last run is shown at the top right. From the first run,

which was used to determine how many eigenvalues existed below 50 Hertz, 93 flexible modes were indicated, and 15 converged modes were found. The next four runs directly above and to the left of the first run in Figure 32 were run simultaneously. From these runs, thirty-four additional converged modes were identified, leaving forty-four that were found in the remaining runs.

At the lowest frequency range, only two modes converged. This is partially due to the fact that there were only two modes in the immediate vicinity of the shift frequency while the other runs had many closely spaced modes near the shift location. However, there were 7 modes between the frequency bounds of V1 and V2 in this low frequency run so that more converged modes were expected. More problems were encountered in obtaining converged modes at the lower frequencies when the lower bound V1 was near the rigid body (zero frequency) modes.

In all of the runs, the value of INIT (number of initially chosen vectors) was set equal to 15. The value of NDYN (number of iterations) was increased from the default value of 8 to values of 13 to 16. With NDYN equal to the default value, the number of converged modes per run decreased considerably in many runs, and this procedure was not considered cost effective for the LDEF model with 1416 degrees of freedom. By examining the runs in Figure 32, the number of converged modes after 8 iterations (NDYN = 8) was tabulated and compared with the converged modes from the computer runs. The results are shown as follows:

Shift Frequency (H_Z)	NDYN in Run	No. of Converged Modes from Run	No. of Converged Modes if NDYN = 8 (default)
7.96	16	2	2
13.96	16	12	12
18.15	15	6	6
20.00	13	12	9
22.51	15	12	6
29.00	15	10	4
35.59	16	13	13
38.98	16	10	5
41.20	15	4	4
43.59	16	11	6
50.00	16	15	9

The increased number of converged modes obtained with an increased number of iterations may be due to the large number of degrees of freedom and the numerous modes with nearly identical frequencies.

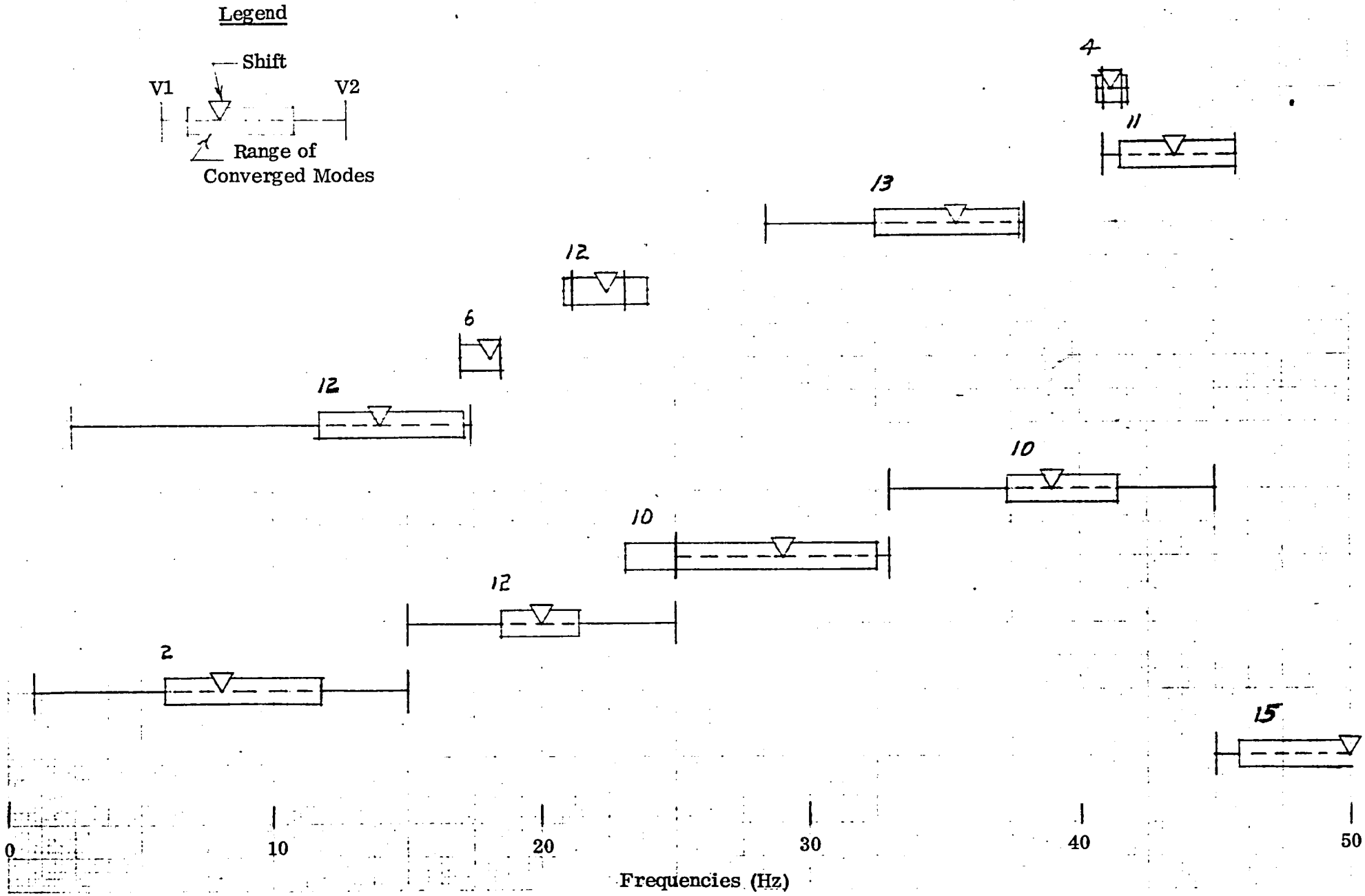

Figure 32. SPAR Eigensolutions for Free-Free Modes of LDEF

REFERENCES

1. W. D. Whetstone, C. E. Jones, R. A. Moore, and C. L. Yen. SPAR Structural Analysis System Reference Manual. System Level 13A. NASA Contractor Report CR 158970-1, 2, 3; Volume 1 - Program Execution, Volume 2 - Theory, Volume 3 - Demonstration Problems; December 1978.

2. Timoshenko, S. and Woinowsky-Krieger, S: Theory of Plates and Shells. Second ed., Mc-Graw Hill Book Co., Inc. 1959.

3. Structural Design Guide for Advanced Composite Applications, Advanced Composites Div., AFML, Wright-Patterson AFB, Ohio, 1969.

1. Report No.	2. Government Accession No.	3. Recipient's Catalog No.
NASA CR-159239		

4. Title and Subtitle	5. Report Date
Vibration Analysis of the Long Duration Exposure Facility (LDEF) Using SPAR	June 1980
	6. Performing Organization Code
7. Author(s)	8. Performing Organization Report No.
Harold Edighoffer	
	10. Work Unit No.
9. Performing Organization Name and Address	
General Electric Company Philadelphia, PA 19101	11. Contract or Grant No. NAS1-14375-15
	13. Type of Report and Period Covered Contractor Report
12. Sponsoring Agency Name and Address	
National Aeronautics and Space Administration Washington, DC 20546	14. Sponsoring Agency Code

15. Supplementary Notes

Langley Technical Monitor: John L. Sewall
Final Report

16. Abstract

This paper presents a structural dynamic modeling of the Long Duration Exposure Facility (LDEF), which is a Space Shuttle payload of passive scientific experiments contained in trays mounted on a large cylindrically shaped structure. Special detailed finite element modeling, using the SPAR system of computer programs, was required to obtain good agreement between analytical and test vibration modes. The scientific experiment trays contributed significantly to overall LDEF stiffnesses, and these contributions were realistically represented for each tray by the stiffness matrix of an equivalent orthotropic panel in the overall LDEF model. Orthotropic stiffnesses for this equivalent panel were obtained from finely detailed statically loaded SPAR models which included stiffness coupling and allowed for partial relative sliding of the tray clamping attachments. Sensitivity to LDEF joint boundary conditions was determined, and static test data proved valuable in assessing modeling of local end fittings.

17. Key Words (Suggested by Author(s))	18. Distribution Statement
Long Duration Exposure Facility Structural dynamic modeling SPAR Vibration analysis	Unclassified - Unlimited Subject Category 39

19. Security Classif. (of this report)	20. Security Classif. (of this page)	21. No. of Pages	22. Price*
Unclassified	Unclassified	95	$6.00

For sale by the National Technical Information Service, Springfield, Virginia 22161